REPORT DOCUMENTATION PAGE

AFRL-SR-AR-TR-06-0455

1. REPORT DATE *(DD-MM-YYYY)*	2. REPORT TYPE	3. DATES COVERED *(From - To)*
	Final Report	01 January 2003 - 31 December 2005

4. TITLE AND SUBTITLE

Active Control of Supersonic Impinging Jets using Supersonic Microjets

5a. CONTRACT NUMBER

5b. GRANT NUMBER

F49620-03-1-0017

5c. PROGRAM ELEMENT NUMBER

6. AUTHOR(S)

Farrukh Alvi

5d. PROJECT NUMBER

5e. TASK NUMBER

5f. WORK UNIT NUMBER

7. PERFORMING ORGANIZATION NAME(S) AND ADDRESS(ES)
Department of Mechanical Engineering
Florida A&M University
Tallahassee FL 32310

8. PERFORMING ORGANIZATION REPORT NUMBER

9. SPONSORING/MONITORING AGENCY NAME(S) AND ADDRESS(ES)
USAF/AFRL
AFOSR
875 North Randolph Street
Arlington VA 2220
Dr John Schmisseur/NA

10. SPONSOR/MONITOR'S ACRONYM(S)

AFOSR

11. SPONSOR/MONITOR'S REPORT NUMBER(S)

12. DISTRIBUTION/AVAILABILITY STATEMENT

Distribution Statement A. Approved for public release; distribution is unlimited.

13. SUPPLEMENTARY NOTES

14. ABSTRACT

A comprehensive experimental investigation on the use of microjets for the control of supersonic impinging jets was conducted under this research program. Supersonic impinging jets occur in many applications including in STOVL aircraft where they lead to a highly oscillatory flow with very high unsteady loads on the nearby aircraft structures and the landing surfaces. Prior research has shown that microjets, placed around the main jet periphery, are very effective in reducing the flow unsteadiness and the associated dynamic loads. In the present work, our goal was to better understand the physical properties of supersonic impinging jets through detailed experiments and to develop optimal open and closed-loop control strategies in order to produce efficient control over the range of conditions impinging jet-related problems are significant.

15. SUBJECT TERMS

16. SECURITY CLASSIFICATION OF:			17. LIMITATION OF ABSTRACT	18. NUMBER OF PAGES	19a. NAME OF RESPONSIBLE PERSON
a. REPORT	b. ABSTRACT	c. THIS PAGE			19b. TELEPHONE NUMBER *(Include area code)*
U	U	U	UU	70	

ACTIVE CONTROL OF SUPERSONIC IMPINGING JETS USING SUPERSONIC MICROJETS

FINAL REPORT

AFOSR GRANT # F49620-03-1-0017

Period of Performance: February 2003 – January 2005

Prepared by
F. S. Alvi & A. Annaswamy

Investigators:

F. S. Alvi (PI), C. Shih and A. Krothapalli
Department of Mechanical Engineering
Florida A&M University and Florida State University
Tallahassee, FL 32310

Anuradha M. Annaswamy (PI)
Department of Mechanical Engineering
Massachusetts Institute of Technology
Cambridge, MA 02139

Executive Summary

A comprehensive experimental investigation on the use of microjets for the control of supersonic impinging jets was conducted under this research program. Supersonic impinging jets occur in many applications including in STOVL aircraft where they lead to a highly oscillatory flow with very high unsteady loads on the nearby aircraft structures and the landing surfaces. Prior research has shown that microjets, placed around the main jet periphery, are very effective in reducing the flow unsteadiness and the associated dynamic loads. In the present work, our goal was to better understand the physical properties of supersonic impinging jets through detailed experiments and to develop optimal open and closed-loop control strategies in order to produce efficient control over the range of conditions impinging jet-related problems are significant.

Through detailed measurements, a better understanding of the flow physics that governs this control strategy was obtained. In particular, the PIV measurements reveal that the activation of the microjets introduces strong and well-organized streamwise vorticity in the jet shear layer. By considering the results of the 2 and 3-component PIV measurements in terms of the vorticity transport equation, there is very strong circumstantial evidence that the streamwise vorticity is primarily due to the redirection of the azimuthal vorticity in the primary shear layer. The cumulative effect of an increase in the shear layer thickness and a decrease of the peak azimuthal vorticity efficiently suppresses the primary shear layer instability, thus attenuates the large-scale structures and upstream propagating acoustic waves. The emergence of three dimensionality due to the streamwise vorticity further disrupts the spatial coherent of the coupling between the acoustic wave and shear layer instability. Combined, these effects lead to the weakening of the

feedback loop, and the subsequent effective, reduction of the overall unsteadiness of the supersonic impinging jet flow. In preliminary, proof-of-concept experiments, microjet control was also implemented in moderately heated jets where it proved to be as equally effective as in controlling cold impinging jets.

A physical model was developed which appears to capture the essential features of the impinging jet flowfield from a controls' perspective. Pulsed actuation concepts were explored in order to obtain more uniform reductions over the entire operating range. An in-house actuator was designed so that the microjets can be temporally modulated thus allowing for more efficient implementation of close-loop control. By pulsing the microjets control effectiveness was significantly enhanced and i) larger noise reductions were achieved at mass flow rates comparable to steady microjets and ii) comparable reductions (relative to steady injection) were obtained with pulsed jets with a significantly lower mass flow rate. These results, especially the continued effectiveness of microjet control for hot jets as well as the opportunity to achieve further performance gains with pulsed actuation suggest that microjet control holds significant promise for practical applications.

1. INTRODUCTION

It is well known that the impingement of a high-speed jet stream on the ground generally results in an extremely unsteady flowfield, which leads to number of undesirable aeroacoustic-related effects. Significant among these are the substantially higher ambient noise levels in the jet vicinity, and very highly unsteady pressure loads on the ground plane and nearby structures. Frequently, the noise and the unsteady pressure spectra are dominated by high-amplitude discrete tones, commonly referred to as impingement tones, which can lead to a marked increase in sonic fatigue. These problems become more pronounced for supersonic impinging jets, the operating regime of the STOVL version of the future Joint Strike Fighter (JSF).

A host of studies on the aeroacoustics of impinging jets by Powell (1953), Neuwerth (1974), Tam and Ahuja (1990) and more recently by Krothapalli *et al.* (1999) have clearly established that the self-sustained, highly unsteady behavior of the jet and the resulting impinging tones are governed by a feedback mechanism. The instability waves in the jet that originate at the nozzle exit grow (into large-scale structures) as they propagate downstream towards the impingement surface; acoustic waves are produced upon impingement of these structures which travel upstream and excite the nascent shear layer near the nozzle exit. For further details of the feedback loop, the reader is directed to the above articles. It is evident that the undesirable effects of supersonic impinging jets need to be controlled in order to minimize their adverse influence on aircraft performance. Although the study of impinging jets has continued to be the focus of current research, the emphasis has more recently shifted on identifying control strategies to reduce the aforementioned adverse effects associated with this flow.

The adverse phenomena associated with impinging jets include severe ***ground erosion*** on the landing surface and ***Hot Gas Ingestion (HGI)*** into the engine inlets (Margason et al., 1997). The presence of multiple impinging jets can potentially further aggravate these effects due to the strong coupling between the jets and the emergence of an upward-moving fountain flow flowing opposite to the lift jets (Elavarasan, et al., 2001). A schematic of a generic STOVL aircraft with multiple lift/impinging jets is shown in Figure 1 where various regions where these problems might occur have been indicated.

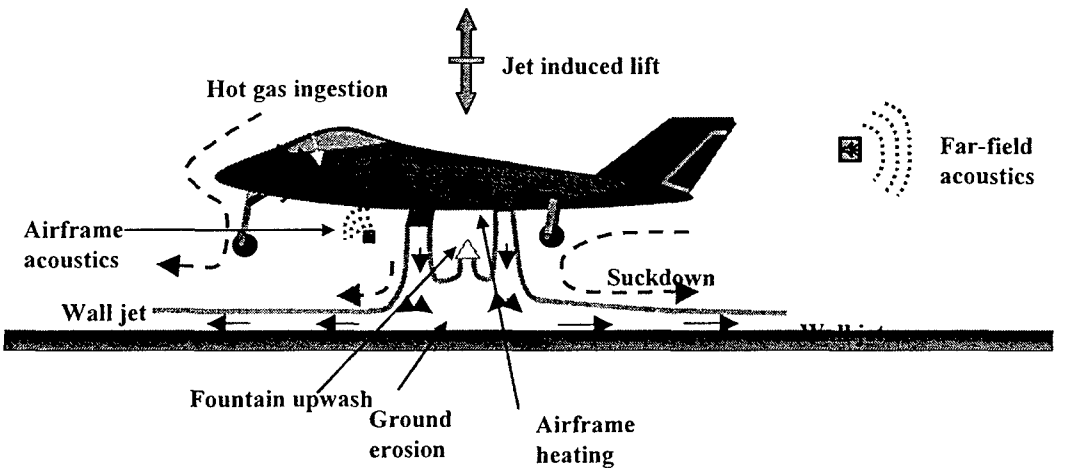

Figure 1 - Flowfield created by the propulsion system around a STOVL aircraft.

A comprehensive study, primarily sponsored by the Air Force Office of Scientific Research (AFOSR), was initiated at the Fluid Mechanics Research Laboratory (FMRL), in Tallahassee, Florida. Using relatively simple configurations, such as that shown in Fig. 2 – consisting of a single jet issuing through a planar, circular plate – the goal of our research is to first obtain a better understanding of the fundamental flow physics involved behind the impinging jet flowfield. Using this knowledge, we have developed and implemented a unique

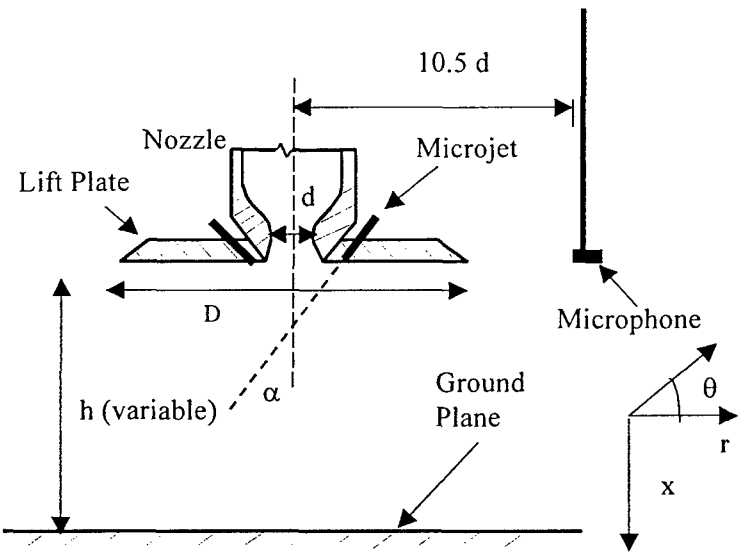

Fig. 2 –Schematic for a single impinging jet experiments.

control technique, which utilizes supersonic microjets and significantly alleviates the ground effect for single and dual impinging jets. Based on detailed velocity and vorticity field measurements along with the measurement of the unsteady pressure field and acoustics we have gained some insight into the main physical parameters governing this control technique. This improved understanding has in turn allowed us to significantly improve the efficiency of our control approach. A physical model which appears to capture some of the dominant features of this flow was developed and compares favorably to experimental results. Finally, in order to further improve the efficiency of microjet control, a pulsed microjet actuator system was designed and tested. In this report, representative results from all these aspects of our research program will be summarized.

1.1 Active and Passive Control– A Brief Summary

The logical approach to controlling the adverse effects of impinging jet flows is to disrupt the feedback loop that is responsible for this unsteady behavior of supersonic impinging jets. A variety of control approaches have been proposed in the literature to accomplish this distruption. One class of control methods attempts to manipulate the shear layer near the nozzle lip to make it less receptive to the acoustic disturbances, thus suppressing the formation of the feedback loop. This concept generally involves a modification of the nozzle geometry and the exit flow conditions using tabs[6] or non-axisymmetric nozzle shapes[7]. Tabs have been shown to eliminate or reduce screech tones, where for some cases, the mixing and shock-associated noise is reduced at lower frequencies but increases at higher frequencies. Using a nozzle with design Mach number of 1.36, Samimy et al (1993) demonstrated that by using 4 tabs, the OASPL was reduced by about 6.5 dB when the jet was operated at an under-expanded mode. However, the reduction in noise was accompanied by a thrust penalty.

Karamcheti et al. (1969) successfully suppressed edge tones in low speed flows, which is governed by a similar feedback mechanism, by placing two plates normal to the jet centerline., Elavarasan et al. (2001) used a similar technique to attenuate the feedback loop in a supersonic impinging jet flow by introducing a control plate just outside the nozzle exit. This passive control method resulted in a reduction in the near field OASPL about 6-7 dB.

Sheplak & Spina (1994) used a high-speed co-flow to shield the main jet from the near field acoustic disturbances. For a suitable ratio of the main jet and co-flow exit velocity, they measured a reduction of 10-15 dB in the near-field broadband noise level in addition to the suppression of impinging tones. However, the very high mass flow needed for co-flow to achieve this makes this approach impractical. Shih et al. (1999) used counter-flow near the

nozzle exit to successfully suppress screech-tones of non-ideally expanded jets. They were also able to obtain modest reductions in OASPL, approximately 3-4 dB while enhancing the mixing of the primary jet.

Although these techniques have shown varied promise, any significant performance gains were confined to a limited range of operating conditions, especially for impinging jets. This is due to the fact that a relatively small change in the nozzle-to-ground separation (h/d) can lead to a significant change in the magnitude and frequency of the tones that are responsible for the undesired flow unsteadiness. Therefore, there is a need for exploring alternate techniques, in particular, ones that do not interfere with the primary nozzle, and also may be amenable to adaptive control.

In the present study, we examine a new technique, which uses a high energy fluid stream to modify the jet shear layer and thus disrupt the azimuthally coherent interaction between the flow instabilities and the acoustic field, was first developed and explored by Alvi *et al* (2003). The proposed control system has the advantage that, depending upon the operating flow conditions, optimal flow control can be achieved by activating the supersonic microjets with the appropriate magnitude and frequency at the desired time instants. In contrast to the traditional passive control methods, the present control-on-demand system can be switched on and off strategically. Therefore, it will not degrade the operational performance of the aircraft when it is not needed. The very small size of the actuator hardware and the minimal mass flow rates requires minimal power consumption and is expected to result in negligible thrust loss of the primary jet. More details regarding this approach is provided next.

1.2 Present Approach – Microjet-based Active Flow Control

Under the current research program, we explored the implementation of a control-on-demand strategy using microactuators in the form of supersonic microjets. These microjets are extremely small and require very low mass flux. In principal, by populating the lift plate at strategic locations, one could develop a system where the most appropriate microjets would be activated to provide optimal control. The proposed control system would in principal achieve optimal flow control by activating the pertinent supersonic microjets with the appropriate magnitude and frequency and at the desired time. In contrast to the traditional passive control methods, the advantage of the proposed on-demand control scheme is that it can be switched on and off as needed. In the present study, microjets were made using 400 μm diameter stainless tubes and which were distributed around the periphery of the nozzle in the nozzle exit plane. A sketch of the microjet arrangement can be seen in Fig. 4; it is discussed in more detail in § 2.

Based on the preceding discussion of the feedback loop, it was anticipated that the array of supersonic microjets may disrupt the feedback loop in number of ways. First, the microjet streams may partially intercept the upstream propagating acoustic disturbances and this attenuates their influence on the shear layer. Second, these high momentum jets can provide spatial/temporal distortions to the coherent shear-layer instabilities thus disrupting their interactions with the acoustic field. Third, the microjet streams may generate streamwise vorticity, which could weaken the downstream traveling large-scale structures thus further weakening the feedback loop.

In Fig. 3, we show a schlieren image of the jet issuing from one of the 400μm micronozzles used in the present experiments. The schlieren image clearly shows that microjet (operating at ~100 psi) flow is supersonic as seen by the characteristic periodic shock-cell structure usually observed in much larger supersonic jets. Judging from the presence of the shock cells, the supersonic core of the jet appears to extend at least 10-12 jet diameters downstream of the nozzle exit. Given the high momentum associated with the supersonic microjets and the large supersonic core length, it is anticipated that they will serve as effective 'actuators' capable of penetrating the primary jet shear layer and modifying its properties. As the results described in section 3 onwards illustrate, this approach was extremely effective in reducing the high noise and unsteady loads associated with supersonic impinging jets. Using

minimal mass flow rates through the microjets, the near-field noise and the unsteady pressure loads were reduced by as much as 12-14 dB.

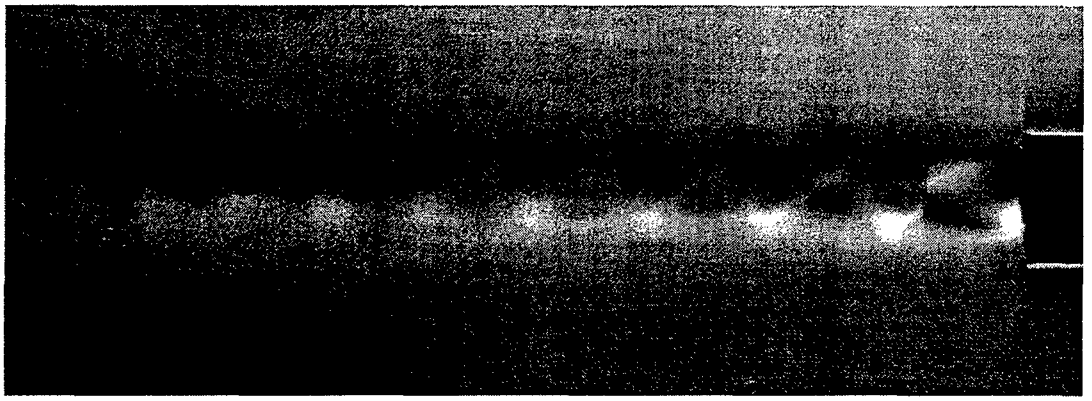

Fig. 3 - Schlieren image of a supersonic microjet issuing from a 400 micron nozzle, $P_0 \sim 100$ psi.

2. EXPERIMENTAL HARDWARE & TECHNIQUES

2.1 Facility and Hardware

The experiments were carried out at the STOVL supersonic jet facility of the Fluid Mechanics Research Laboratory (FMRL) located at the Florida State University. This facility is used primarily to study jet-induced phenomenon on STOVL aircraft hovering in and out of ground effect. Further details can be found in Krothapalli *et al.* (1999). The schematic illustrating a single impinging jet is shown in Fig, 2 and a picture of the facility including a close-up of the lift plate with the microjets is shown in Fig. 4.

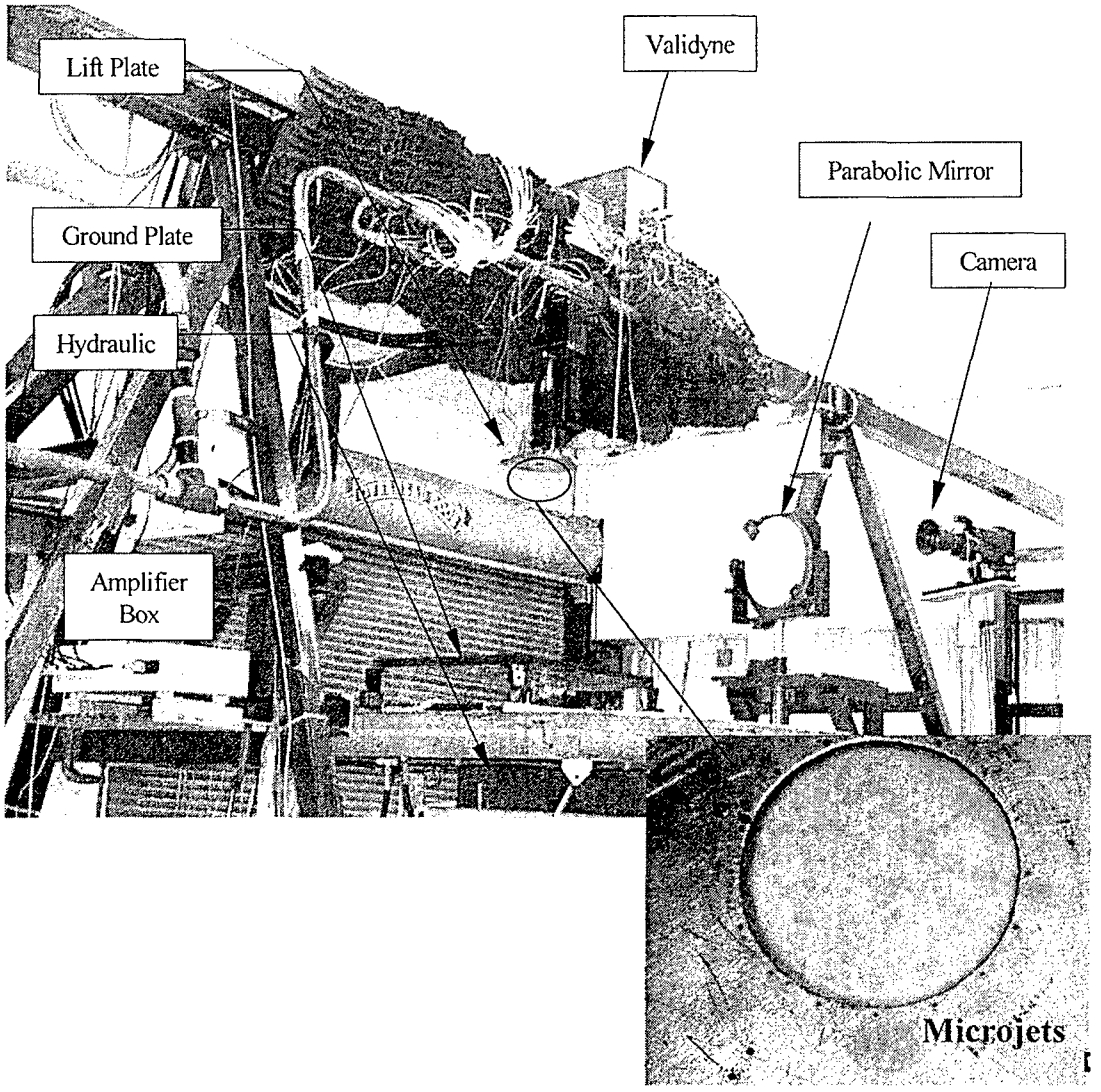

Figure. 4 – STOVL test facility with a close-up view of the Lift Plate with Microjets.

The experiments described herein were conducted using an axisymmetric, convergent-divergent (**C-D**) nozzle with a design Mach number of 1.5. The throat and exit diameters (**d, d_e**) of the nozzle are 2.54cm and 2.75cm (see Figs. 1 & 2). The divergent part of the nozzle is a straight-walled conic section with a 3° divergence angle from the throat to the nozzle exit. Although tests were conducted over a range of Nozzle Pressure Ratios (NPR, where NPR = stagnation pressure/ambient pressure), the results discussed in the present paper are limited to NPR = 3.7 and 5. NPR = 3.7 corresponds to an ideally expanded Mach 1.5 jet, while NPR = 5 produces a moderately under-expanded jet. A circular plate of diameter D (25.4 cm ~10d) was flush mounted with the nozzle exit. The circular plate, henceforth referred to as the 'lift plate', represents a generic aircraft planform and has a central hole, equal to the nozzle exit diameter, through which the jet is issued. A 1m x 1m x 25mm aluminum plate serves as the ground plane and is mounted directly under the nozzle on a hydraulic lift. In order to visualize the flow field in the cross plane of jet the center part of ground plane was replaced by a glass plate for these experiments. Single or dual CCD cameras were mounted under the ground plane, beneath this window, to record the jet cross-plane, Planar Laser Scattering (PLS) images and the PIV images discussed in the Results section.

The main controlling parameter in the experiment was the ground plate height h with respect to the nozzle exit; this was varied from $2d$ to $60d$. The experiments were conducted over a range of NPR. The jet stagnation temperature was maintained at 20°C ± 2°C. The nominal exit Reynolds number at exit of the nozzle was $7x10^5$ (based on exit velocity and nozzle diameter).

Active flow control was implemented using sixteen microjets, flush mounted circumferentially around the main jet as shown in Fig. 2. The jets were fabricated using 400μm diameter stainless tubes and were oriented at approximately 20° or 90° with respect to the main

jet axis. The air supply for the microjets was provided from compressed Nitrogen cylinders through a main and four secondary plenum chambers. In this manner, the supply pressures to each bank of microjets could be independently controlled (see Alvi et al. 2003, included as *Appendix A* , for details). The microjets were operated over a range of NPR = 5 to 7, where the combined mass flow rate from all the microjets was less than 0.5% of the primary jet mass flux. Note that the Figs. 4 and 5 show the arrangements for steady microjets; the pulsed microjet actuators are discussed in § 6.

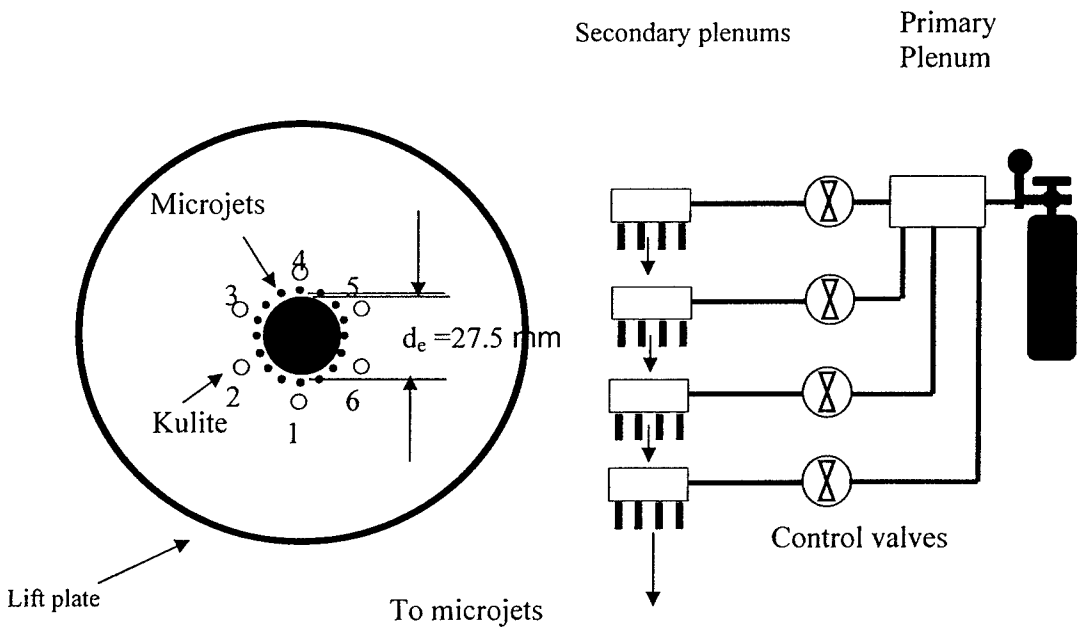

Fig. 5- Schematic of the flow control arrangement using microjets

2.2 Measurement Techniques

The unsteady loads generated by the impinging jet flow were measured using high frequency response miniature Kulite™ transducers on the lift plate and the ground plane. For the lift plate, three transducers (Model XCS-062) were mounted, 35mm, 45mm and 58mm, respectively, away from the center of nozzle. Since the signal measured by all three Kulites on the lift plate depicts similar trends, unless otherwise noted, only data from the Kulite closest to the nozzle is shown in this paper. The unsteady pressure field created by the jet impingement on ground plane was measured with three high frequency Kulite pressure transducers (Model XCQ-062, 100psia) with the data from the Kulite located on the jet centerline shown in this report. In addition, near-field noise was measured using ¼ inch diameter B&K™ microphones placed approximately 25 cm away from the nozzle exit, oriented 90° to the jet axis (see Fig.1). In order to minimize sound reflections during the near-field acoustic measurements, near-by exposed metal surfaces were covered with 10cm thick acoustic foam.

The microphone and the unsteady pressure signals were acquired through National Instruments digital data acquisition cards using the LabView™ software. For unsteady measurements, i.e. microphone and Kulite pressures, 100k points were recorded for each signal. Standard statistical analysis techniques were used to obtain the spectral content and the Over All Sound Pressure Level (OASPL) from these measurements. The spectral content of the unsteady signals was obtained by segmenting each data record into 100 subgroups with 1k points each and an FFT with a frequency resolution of 68.4Hz was computed for each segment. The 100 FFT's thus obtained were averaged to obtain a statistically reliable estimate of the narrow-band noise spectra. The estimated uncertainty associated with the unsteady lift plate pressure, P_{rms}, is ± 0.02

psi while the rms intensities of the ground plane pressures was estimated to be accurate within ± 0.2 psi. The microphone signal was measured with an estimated uncertainty of ± 1 dB.

The flow was visualized using a conventional single-pass shadowgraph in a z-type arrangement. A stroboscopic white-light flash unit with variable pulse frequency of up to 1 kHz was used as a light source. Cross flow shear layer characteristics was examined by a laser sheet illumination visualization technique. Laser sheet, generated by a Spectra Physics Nd-YAG pulsed laser, was projected normal to the primary jet axis. Light scattered by the condensed water droplets in the mixing region renders the shear layer visible and these PLS images were recorded by a CCD camera. In order to obtain stereoscopic PIV measurements, the central portion of the ground plane was replaced by glass plates for these experiments. A single CCD camera was mounted under the ground plane, to record the jet cross-plane, Planar Laser Scattering (PLS) images. The PLS images are not presented in this report; they have been discussed in some detail in Lou et al. (2006) which has been attached as Appendix B. Two CCD cameras were mounted under the ground plane, beneath this window (see Fig. 6), and were used to record the stereoscopic PIV images presented later in this paper. More details regarding the PIV arrangement are discussed in §2.3.

2.3 Particle Image Velocimetry

Particle Image Velocimetry (PIV), was used to obtain whole-field velocity data. The velocities were first measured in the streamwise central plane of the jet using a planar or 2D PIV system and when required, a stereoscopic PIV was used to obtain the three-dimensional velocity field data at several selected downstream locations. The schematic of the experimental arrangement for the stereoscopic PIV system is shown in Fig.6.

The primary jet was seeded with small (~0.3μm) oil droplets generated using a modified Wright Nebulizer. The ambient air was seeded with smoke particles (~1-5μm) produced by a Rosco 1600 fog generator. A double-pulsed Nd:YAG laser (Spectra-Physics, 400 mJ) was used for flow field illumination. A light sheet, ~ 1-1.5 mm thick, was created using a combination of spherical and cylindrical lenses. The stereoscopic PIV setup is based on the stereoscopic approach and two SharpVison^{TM} Model 1400DE cameras consisting of Progressive Scan Interline CCD sensor (SONY ICX 085AL) were used to capture the images as shown in Fig. 6. Each camera has a resolution of 1280 (H) × 1024 (V) active pixels of size of 6.7 × 6.7 μm. The planar PIV images were recorded by a cross-correlation CCD camera (Kodak ES 1.0) with 1k × 1k resolutions. The PIV images were acquired at a rate of 15 image pairs per second. The time between pulses was optimized at 1~1.5 μs depending on the jet operating condition.

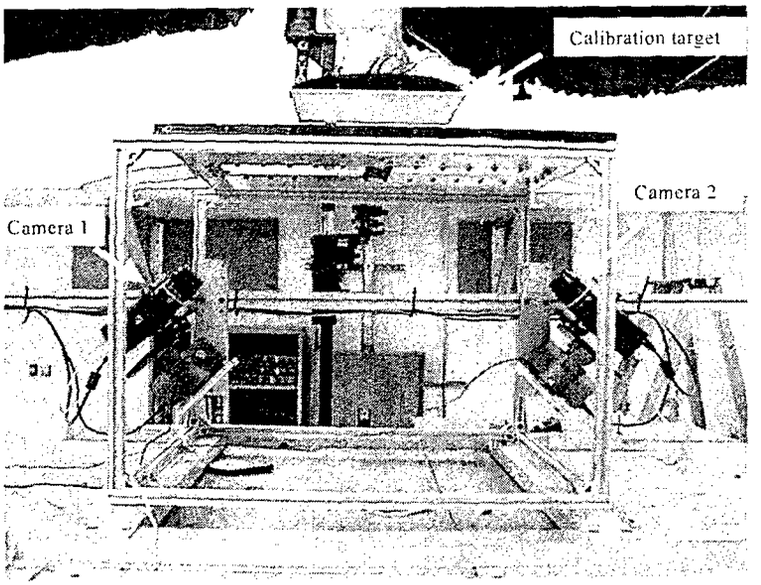

Fig. 6a – Experimental set up for the 3-component PIV system

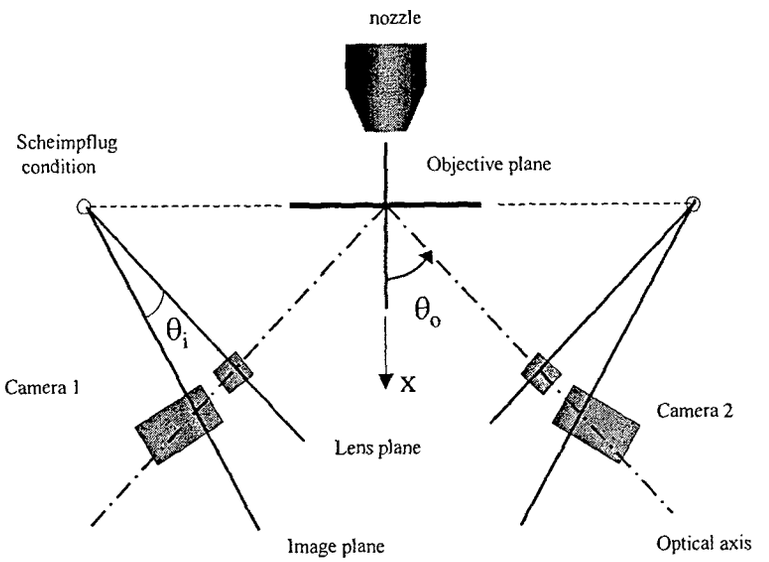

Fig. 6b - Scheimflug Condition for the 3-component PIV system

3. STEADY MICROJET CONTROL OF A COLD JET

3.1 Brief Summary of Earlier Microjet Control Studies

It has been clearly demonstrated in earlier studies (Alvi et al., 2003) and that the use of microjets is effective in reducing both the impinging tones and the overall noise level for supersonic impinging jets. The key results from our previous work will be briefly summarized in the following to provide the background and context for the present research that is continuing in the same area. Fig. 7 shows representative images for the impinging jet flowfield at h/d=4, with and without control. The presence of multiple, strong acoustic waves, marked in the instantaneous shadowgraph for the uncontrolled case, i.e. microjets off, clearly signify the presence of acoustic tones. The emergence of large-scale structures in the shear layer, which are responsible for the generation of acoustic tones upon impingement on the ground plane, is also evident in this picture. Furthermore, the enhanced entrainment associated with such structures is also thought to be responsible for the 'lift loss' suffered by STOVL aircraft during hover (Krothapalli et al., 1999, Alvi et al, 2003). The instantaneous shadowgraph in Fig. 7b shows the visual effect of microjet control on this flow. The effect is visually dramatic: the large-scale structures have been significantly reduced when the microjets are on and this is accompanied by an almost complete disappearance of the strong acoustic waves in the near-field. Also visible in Fig. 7b are the 'streaks' generated by the supersonic microjets. It is worth noting that such streaks are very similar to those generated by tabs (Samimy et al., 1993) and tapes (Krothapalli et al., 1998) and have been taken as an indicator of the presence of streamwise vorticity. We therefore speculated that the production of streamwise vorticity may in part be responsible for the reduction in the flow unsteadiness, which is explored in detail in a later section.

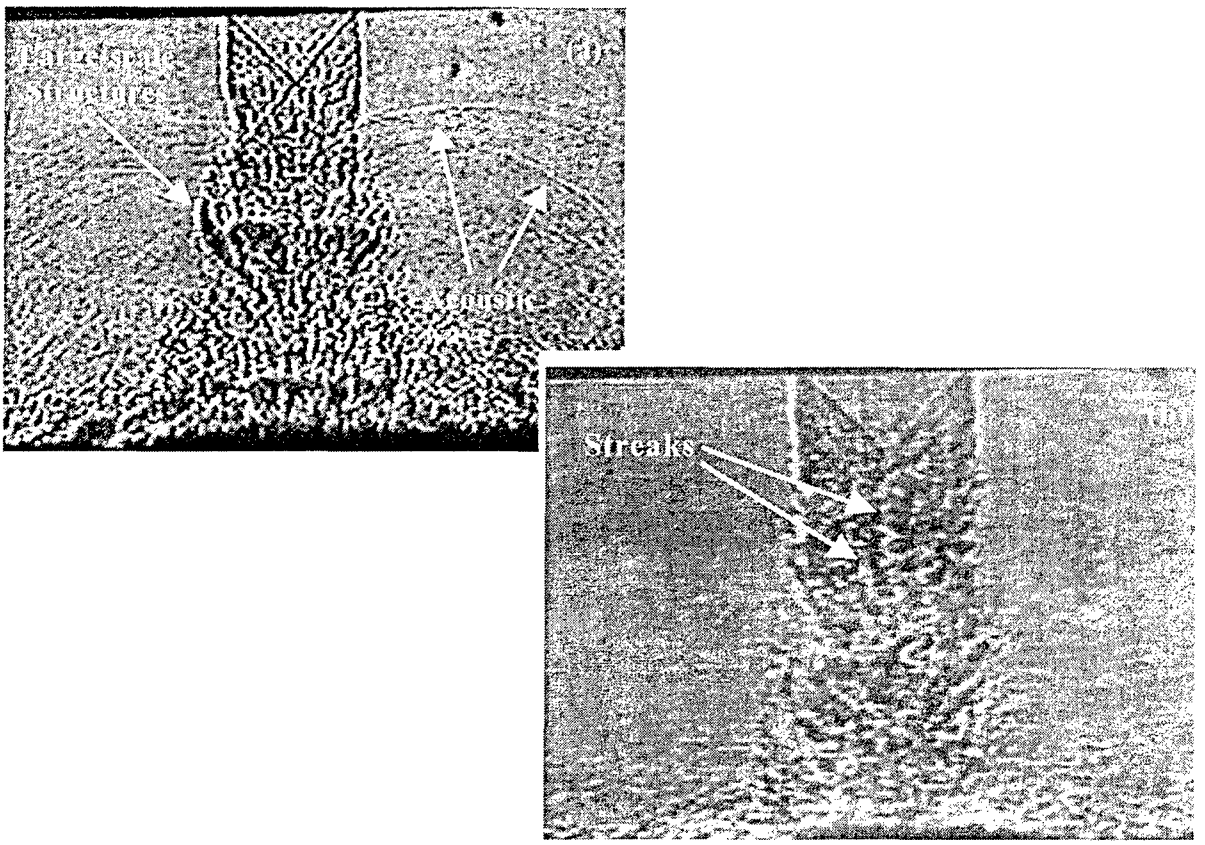

Fig. 7 Instantaneous shadowgraph images, NPR=3.7, h/d=4; (a), No Control; (b), With Control.

Fig. 8 shows the narrow band spectra for the unsteady pressure on the ground plane and the near field noise for NPR 3.7, h/d=4 from two different experiments, where Fig. 8a corresponds to the use of 90° microjets and Fig. 8b to the 20° microjets. Upon comparing the uncontrolled data (solid lines) to the controlled case (dashed lines), one observes that the distinct tones present in the uncontrolled impinging jet are either entirely eliminated or significantly diminished by the activation of microjets. In addition, and perhaps more significantly, the attenuation in the discrete tones is accompanied by a broadband reduction in the spectral amplitudes. This broadband reduction is observed for all spectra due to lower acoustic and pressure fluctuations, which indicates an overall decline in the unsteadiness of the flow when control is implemented.

Plots summarizing the overall reduction in the unsteady pressure levels (P_{rms}) on the lift plate, the ground plane, and in the near-field noise are shown in Figs. 9 and 10 for NPR = 3.7 and 5, respectively. Although a range of microjet pressures were tested, the data shown in these plots correspond to the microjets operating at ~ 100 psi, where the trends observed here are very similar to those obtained at other microjet pressures. These plots clearly show that the fluctuating loads are significantly reduced at all three measurement locations for both NPR's, at almost all heights. However, the magnitude of reduction is strongly dependent upon the ground plane distance (h/d) and to a lesser degree on the nozzle pressure (NPR).

In general, the microjets are more effective for the under-expanded jet (NPR=5) where the lift and ground plate pressures are reduced by 10-14 dB and the near-field noise by 5-6 dB. However, for a given NPR, the magnitude of reduction is strongly dependent upon the ground plane distance (h/d). The variation of the level of reduction appears to have a 'staging' behavior as seen in Fig. 9. This trend of non-uniform reductions for the microjet control might be related to the well-known staging behavior of the impingement tones with ground plane distance. The non-uniform reduction suggests that efficient control of this flow requires an adaptive control approach where the microjets need to be manipulated to provide optimal control at all heights. This non-uniform behavior is the reason for exploring various adaptive control approaches discussed in sections 5 and 6.

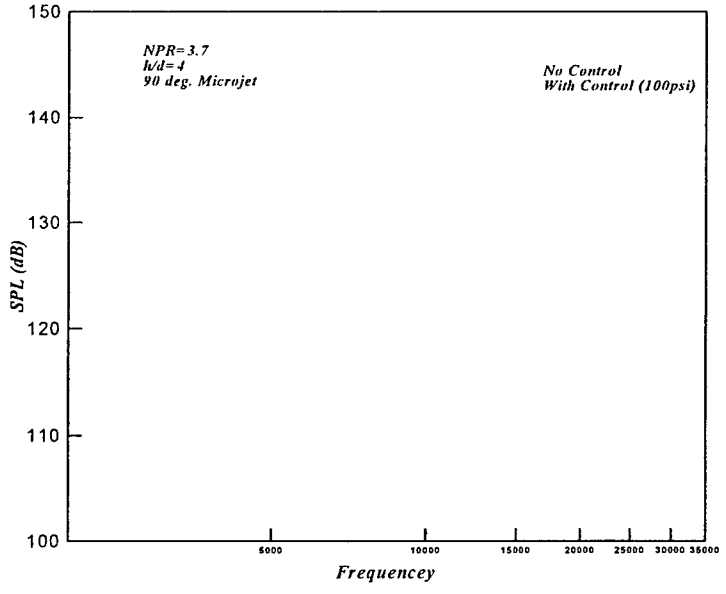

Fig. 8a Near field noise spectra, NPR=3.7, h/d=4, 90 deg. microjet

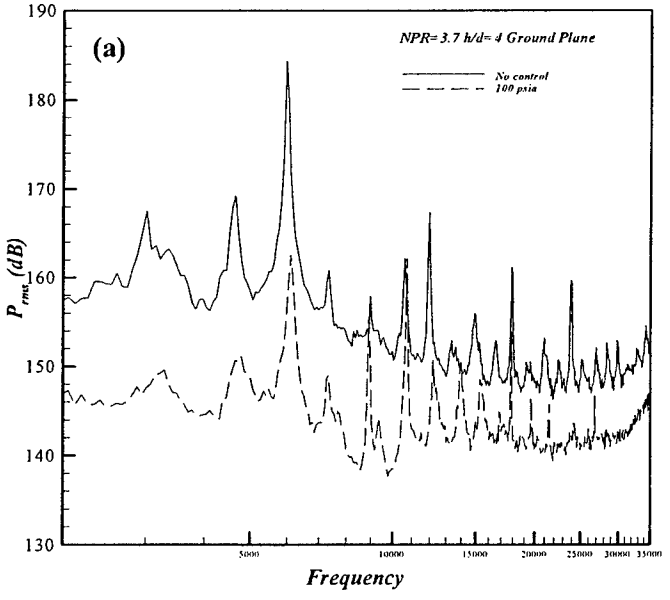

Fig. 8b Unsteady spectra on the Ground Plane NPR=3.7, h/d=4, *20 deg.* microjet

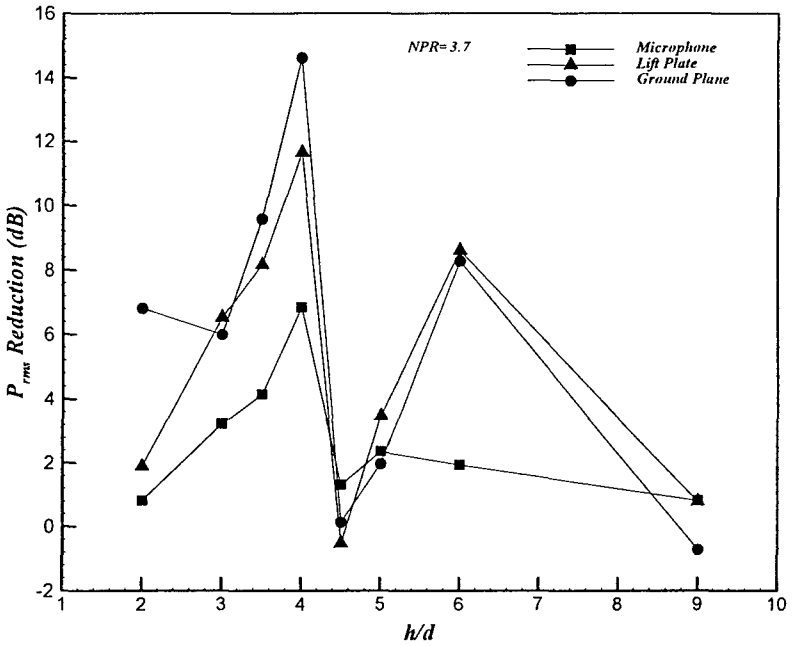

Fig. 9 Reductions in fluctuating pressure intensities as a function of h/d, NPR=3.7, 20° microjets.

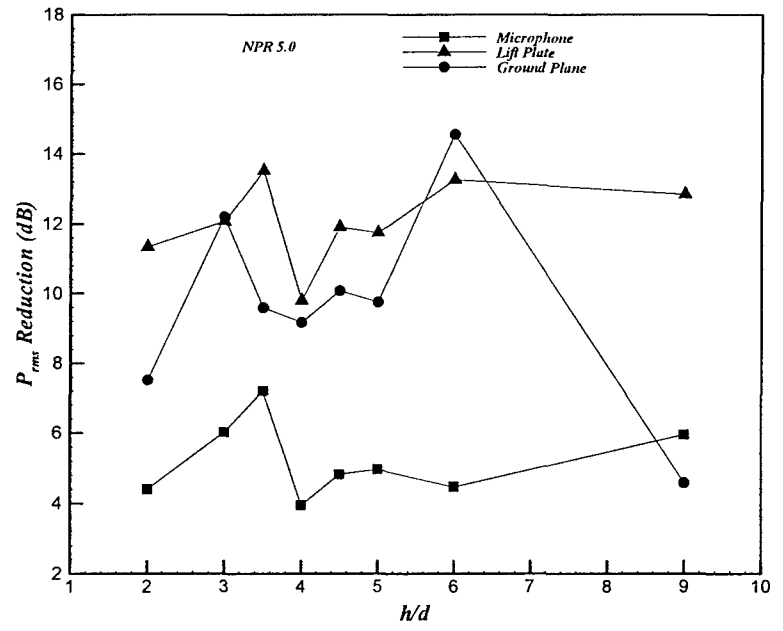

Fig. 10 Reductions in fluctuating pressure intensities as a function of h/d, NPR=5, 20° microjets.

3.2 Parametric Effects Using Steady Microjets

A comprehensive parametric study, examining the effect of microjet control parameters and configurations on the overall flow control efficacy was conducted in order to determine the optimum operating conditions – in terms of noise reduction - using steady microjets. These experiments, which cover a large parametric space, also provide some insight on the physical mechanisms behind the microjet control technique. With this in mind, the parameters varied include: the microjet operating pressure, microjet angle, the use of micro-tabs instead of microjets, microjet size, the number/spacing of microjets, and spatial distribution of microjets relative to the main jet. Only the effect of microjet angle and pressure is briefly described next; more details regarding these parametric effects can be found in Lou et al. (2006).

Microjet Angle

The first parameter examined is the microjet angle with respect to the main jet flow. The microjet operating pressure is fixed at 100 psi for the results discussed in this subsection. It has been shown (Alvi et al., 2003) that the 20° microjet is more effective for under-expanded conditions relative to ideally- and over-expanded cases. It was first thought that this difference was due to the concave curvature of the jet boundary when the jet is operated at under-expanded conditions. The emergence of a concave jet shear layer at the nozzle exit makes it easier for the microjet streams to perturb the primary shear layer.

For the ideally expanded case shown in Fig. 11, the noise reduction due to microjet control is improved for almost all heights when the angle is changed from 20° to 90°. This increase in the control efficacy is quite substantial where the unsteady pressures on both the lift and ground planes are further reduced by 5 to 8 dB relative to the 20° microjets. The change is

even more dramatic at certain heights, such as h/d=2, 4.5, 5, which show minimal reduction with the 20° microjets. Recalling that the 90° microjets do not intercept the acoustic waves, but still manage to provide more effective control than 20° microjet clearly indicates that the shielding from, or the interception of, the acoustic waves by the microjet streams is not the primary mechanism behind this control scheme.

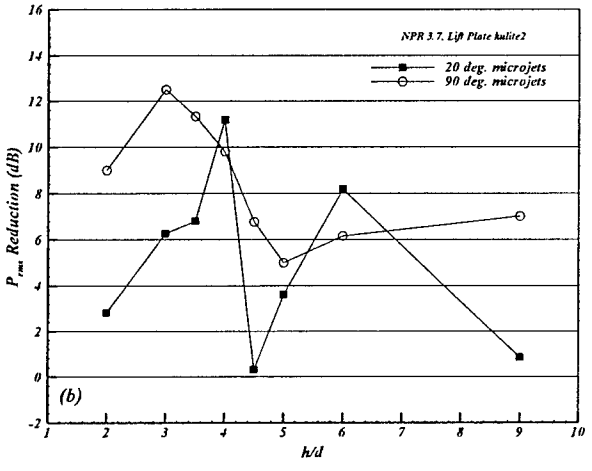

Fig. 11- Reductions of fluctuating pressure intensities, NPR=3.7, 20° verse 90° microjet control;

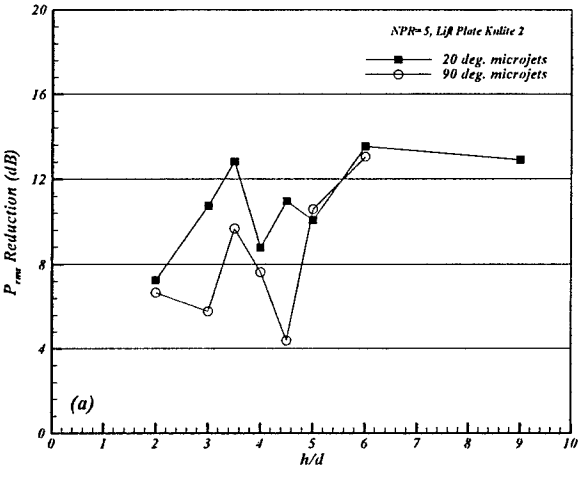

Fig. 12- Reductions of fluctuating pressure intensities, NPR= 5, 20° verse 90° microjet control;

In contrast, the trends observed in Fig.12 are the opposite of those seen in Fig. 11. For the under-expanded case shown in Fig. 12, the attenuations due to the 90° microjets are somewhat smaller at almost all the heights when compared to the noise reduction efficacy for the 20° microjets. However, an examination of the OASPL data without control for NPR=5 indicates that this apparent difference in control efficiency is primarily due to the difference in the unsteady pressure levels for the baseline (uncontrolled) case, i.e. between the 90° and 20° configurations. As seen in Fig. 13, whereas the values are almost identical for the baseline/no-control condition for the two microjet inclinations at NPR =3.7 (Fig. 13a); for the under-

expanded condition (NPR=5, Fig. 13b) the baseline Prms is significantly lower for the 90° microjet configuration. Since the Prms values with control are very similar for the 20° microjets and 90° microjets (Fig. 13b), the *net reduction* with the 90° microjets is lower due to lower baseline values. The reason behind this apparent discrepancy in the baseline Prms values is due to the fact that 90° micro-nozzles protrude into the jet shear layer for the NPR=5 underexpanded jet, thus acting as microtabs and thus reducing passively the baseline noise. (See Lou et al. 2006 for more details)

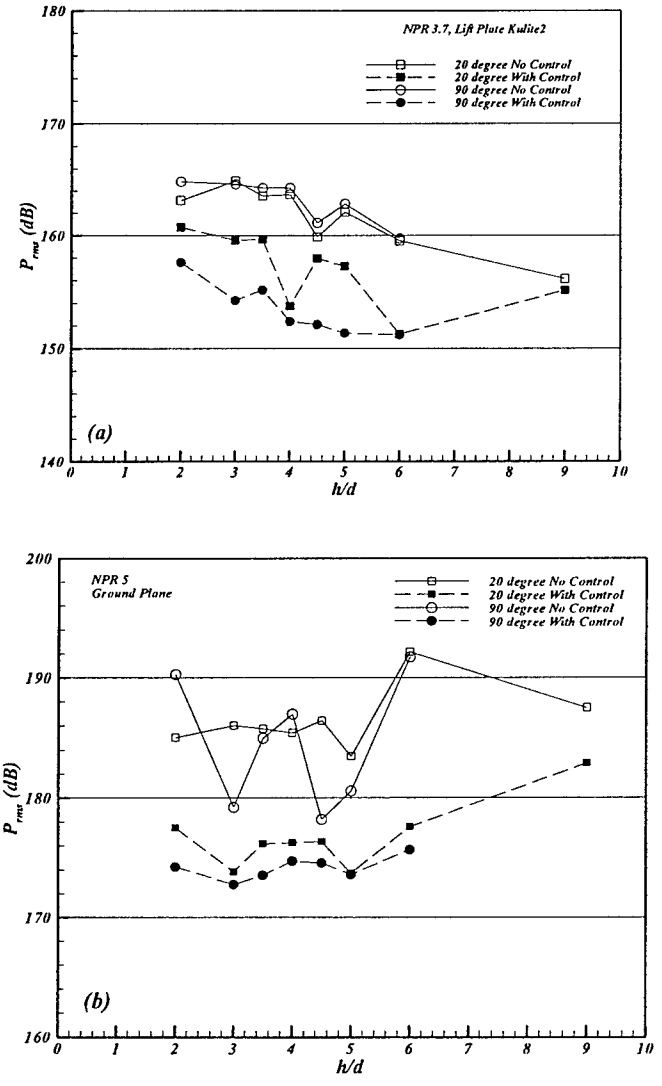

Fig. 13 - Unsteady pressure intensities; (a), NPR=3.7, Lift Plate; (b), NPR=5, Ground Plane.

Microjet Pressure

The "penetration depth" of the microjet stream into the primary jet shear layer is also a parameter expected to contribute to the efficacy of microjet control. It has been shown (Phalinkar, et al, 2001) that a stronger microjet stream with a longer supersonic core length can be generated if the microjets are operated at a higher stagnation pressure. Consequently, the effect of microjet pressure on control efficiency was examined. The effect of this parameter on the reduction in dynamic pressures is shown in Fig.14 and Fig.15.

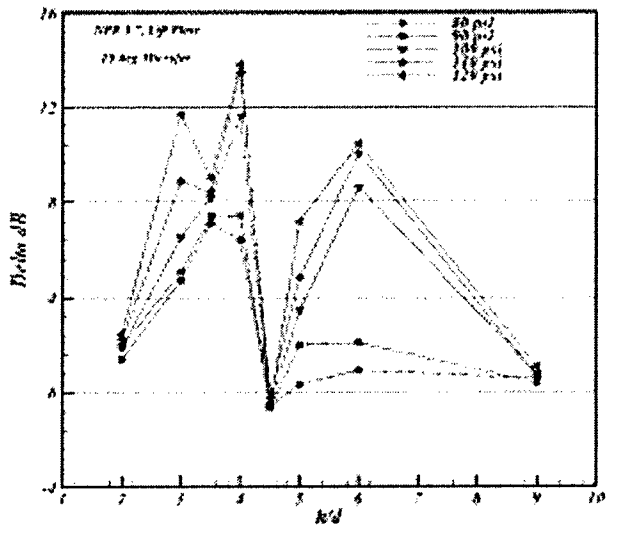

Fig. 14 - Effect of Microjet Pressure on Prms at NPR=3.7 using 20° microjets.

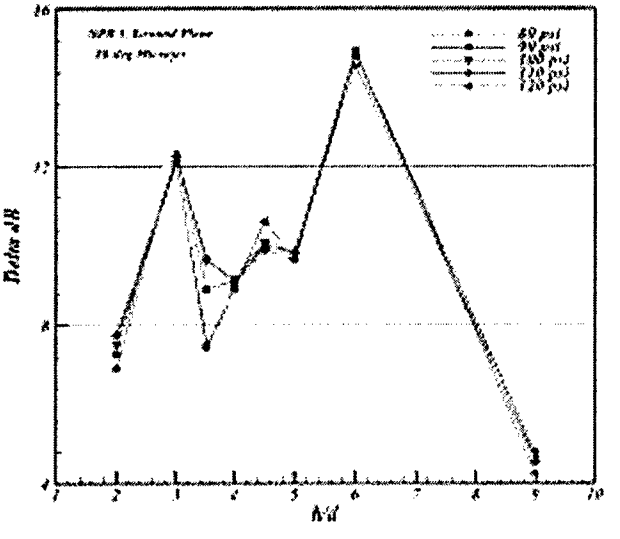

Fig. 15 - Effect of Microjet Pressure on Prms at NPR=5 20° microjets

For the results shown here, the microjet pressure is increased from 80 psia to 120 psia in increments of 10 psi. For the ideally expanded case shown in Fig. 14, the reductions in P_{rms} increase relatively fast as the microjet pressure is increased from 80 to 100 psia. Beyond this value, the gains in performance, i.e. in reducing Prms, become increasingly small at most heights. For the present study, the performance of the 20° microjets is near saturation at

approximately 100 psi. Hence, in terms of performance, increasing the pressure beyond 100 psi yields very little dividends.

The results are somewhat different when the primary jet is operating at an under-expanded condition as shown in Fig.15. As seen here, increasing the microjet pressure from 80 to 120 psi has a negligible effect on performance. This is because saturation in performance occurs at pressures below 80 psi, roughly around 50-60 psi, for the under-expanded case. These results indicate that increasing the pressure significantly above saturation levels does not change the system behavior and lead to any further performance gains.

4. PHYSICAL MECHANISMS – THE VELOCITY & VORTICITY FIELD

To better understand the impinging jet flowfield and more importantly to examine the effect of microjets on this flow, extensive PIV measurements were carried out over a range of conditions. These include, planar 2-component, PIV measurements in the streamwise central plane of the jet and at various cross-sectional planes (normal to the jet axis). In addition, 3-component PIV measurements were also obtained for selected conditions and locations using a dual camera PIV system. These measurements, and the understanding gleaned therein, are discussed in this section.

4.1 Properties of the Primary Jet Shear Layer

A contour plot of the mean velocity distribution is shown in Figs. 16 and 17 for NPR 3.7 and 5, respectively, where, velocity vector profiles are superimposed at selected streamwise locations. These plots are obtained by averaging data from 400 instantaneous PIV whole-field measurements, thus providing a reliable estimate of the mean velocity field Ideally, the jet with design a Mach number 1.5 should be shock-free at NPR=3.7, which corresponds to the ideally expanded condition. A weak periodic shock-cell structure is seen in the velocity contour plots in Fig. 16a, in part due to the enhanced entrainment of the ambient air into the jet, which generates a low pressure on the lift plate and in the vicinity of the nozzle exit (Krothapalli et al., 1999). This results in a very weakly underexpanded jet at the nozzle exit, as seen in these velocity contour plots.

At NPR=5, a moderately under-expanded jet, the shock cell structures is more clearly evident Fig. 17. The shock cell spacing can easily be measured from the identifiable peaks and valleys in the velocity distribution along the centerline of the jet. A comparison of the baseline flow, to the corresponding control cases shows that although the unsteady flow behavior has

been drastically modified with the introduction of microjets, the jet velocity field is not significantly altered, at least qualitatively. This in turn suggests that the jet propulsion properties are not substantially altered by the microjet control, an important consideration for a scheme that can be implemented in a real system.

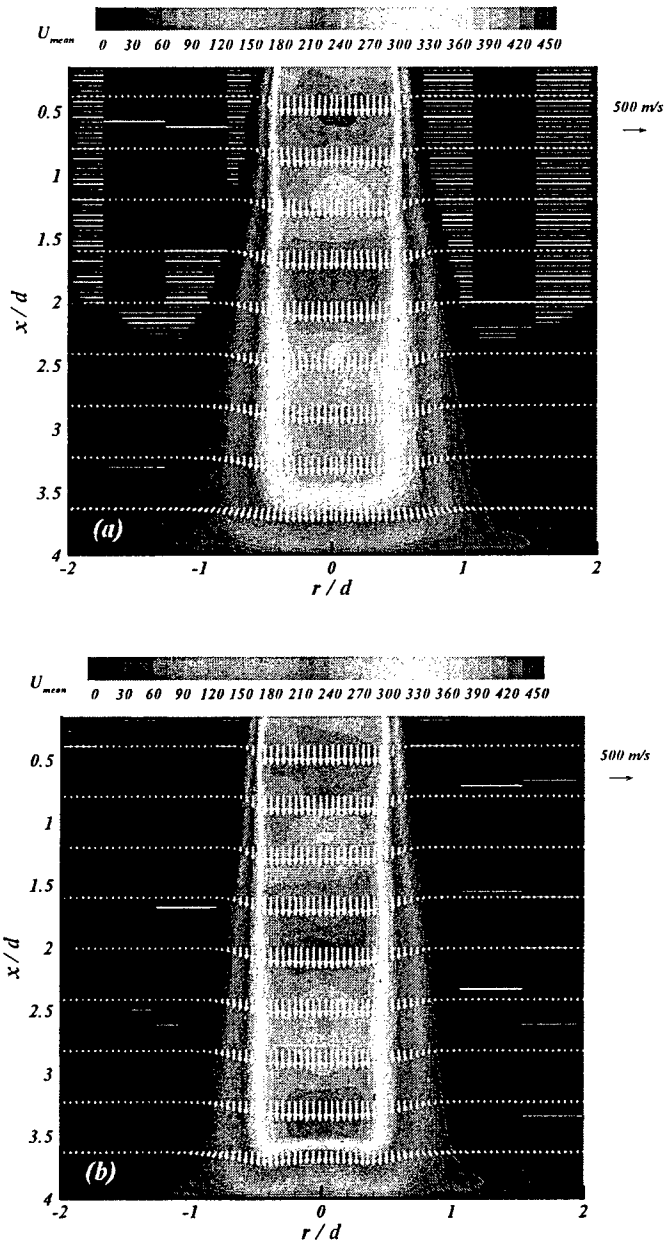

Fig. 16 - *Ensemble-averaged* streamwise velocity distribution at center plane of the jet flow, NPR=3.7, h/d=4. (a) No Control; (b) With Control

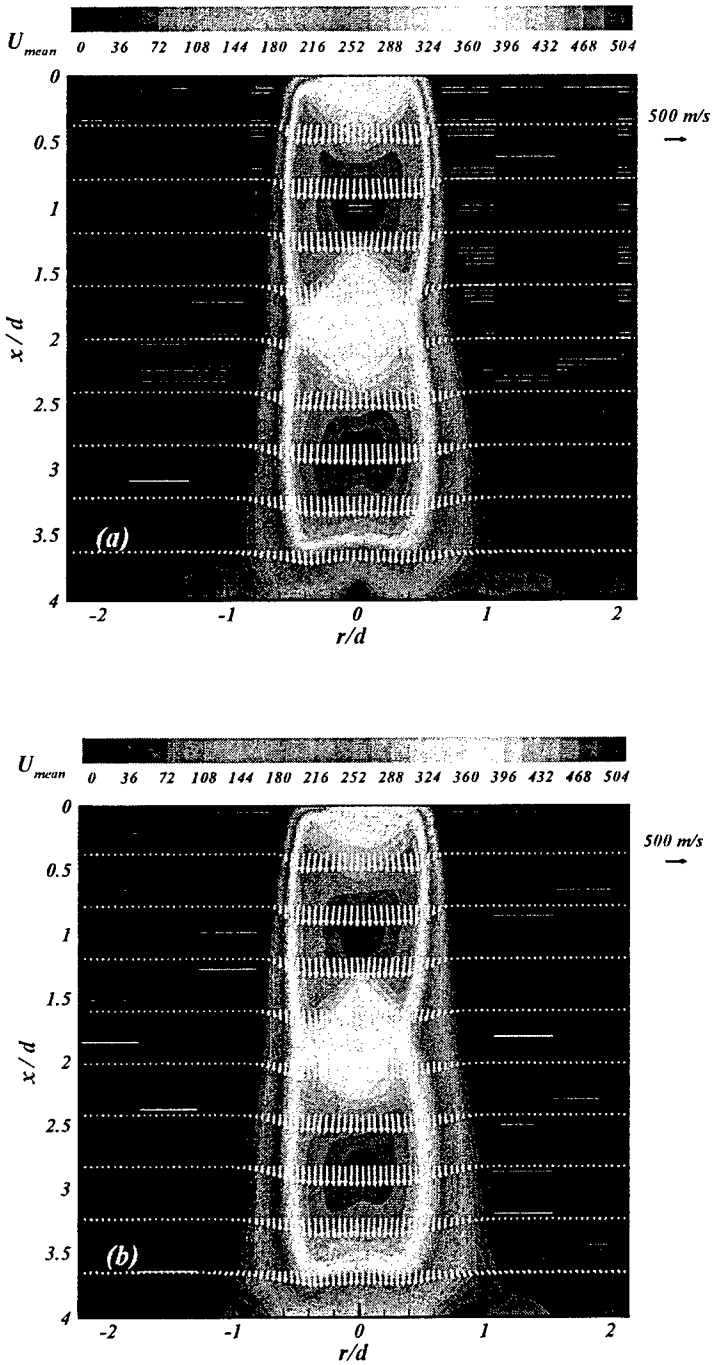

Fig. 17 - *Ensemble-averaged* streamwise velocity distribution at center plane of the jet flow, NPR=5, h/d=4. (a) No Control; (b) With Control

Since the initial shear layer growth has a significant effect on the overall instability, we closely examine the influence of the microjet control on the shear layer characteristics for a better understanding of the physical mechanism behind the present control scheme. To quantify the growth of the shear layer, the shear layer width, δ, is defined as $\delta = r_{0.1} - r_{0.9}$; here $r_{0.1}$ and $r_{0.9}$ are the radial locations where the local mean velocities reaching 10% and 90% of the local jet center line velocity, respectively. Based on this definition, a plot of the shear layer thickness, extracted from the velocity field data, is shown in Fig. 18 as a function of x/d for both the baseline and the microjet controlled case. Two noteworthy observations can be made here: First, the shear layer with control is thicker initially as compared to the no control case. The thickening of the jet boundary layer has been related directly to the emergence of strong streamwise vortices due to the microjet control. The increase of the shear layer thickness in the initial region can reduce the receptivity of the shear layer and limit the number of unstable modes. This may directly lead to the second observation that the shear layer grows more slowly when control is on. This is also be explained by the earlier observation that the suppression of the feedback loop by microjets significantly stabilizes the overall flow behavior (Alvi et al., 2003).

As discussed earlier, flow unsteadiness is reduced with increasing microjet pressures. Hence, we explore the response of the primary jet shear layer growth with microjet pressure in Fig. 19. This plot clearly illustrates that the variation of the shear layer growth rate is inversely related to the microjet pressure. That is, a decrease in the shear layer growth rate leads to a corresponding increase in the reduction in the flow unsteadiness. Both trends asymptote towards constant levels beyond the established threshold control pressure (>40 psia). To summarize, this evidence clearly suggests that the reduction in the flow unsteadiness due to microjets is at least in

part due to the thickening of the initial shear layer in the primary jet which in turn makes it more stable and less susceptible to perturbations due to the feedback loop.

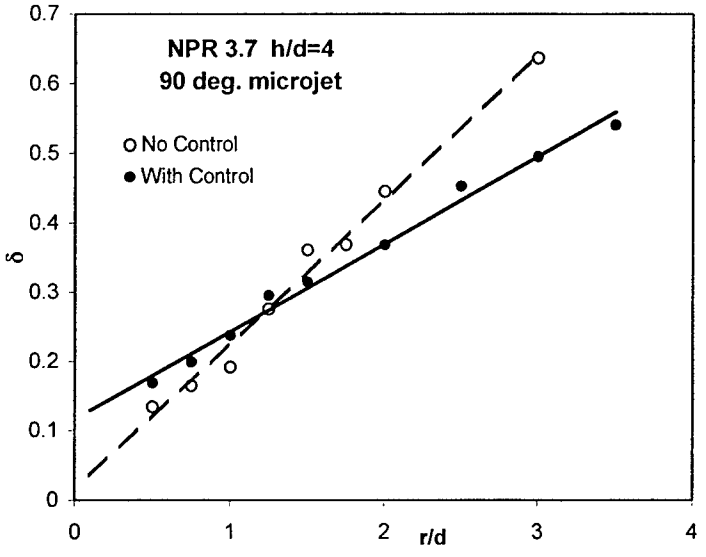

Fig. 18 - Streamwise variation of shear layer thickness, NPR=3.7, h/d=4, 90° microjet @ 100 psia

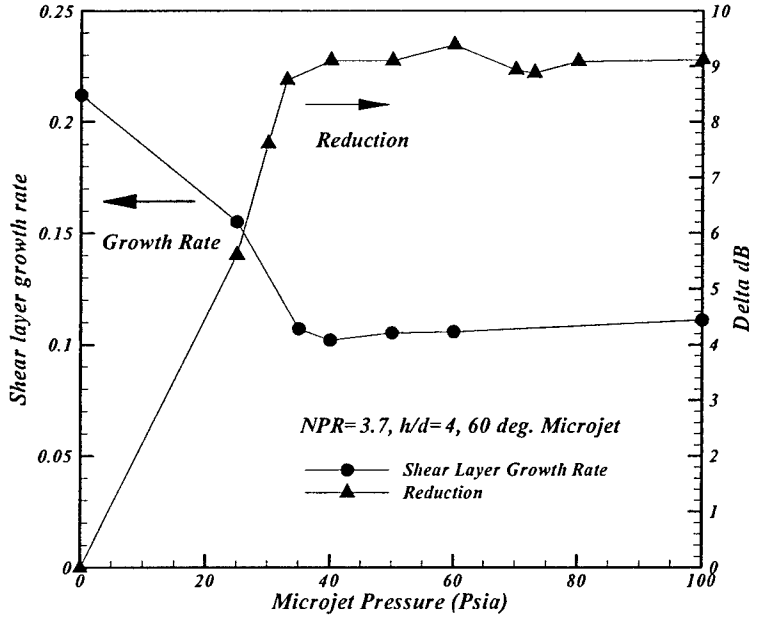

Fig. 19 - Effect of microjet operating pressure on shear layer growth rate NPR=3.7, h/d=4

4.2 The Azimuthal Vorticity Field

The flow visualization results clearly demonstrate that microjet control effectively disrupts the feedback loop leading to the suppression of the large scale vortical structures typically observed in uncontrolled impinging jets. Consequently, a study of the vorticity fields with and without control is expected to provide a better understanding of the fundamental mechanisms behind this control.

An examination of the *ensemble-averaged* vorticity contour plots in the jet central plane (not shown here) reveals that the azimuthal vorticity is much weaker when microjets are activated. To investigate this further, the peak value of the locally normalized azimuthal vorticity, $(\Omega_\theta d/U_j)_{\max}$ has been plotted as a function of x/d in Fig. 20. As expected, the peak vorticity decreases gradually as the jet expands downstream for both cases shown here. Moreover, the peak values are *lower with microjet control at all streamwise locations* for both ideally and under-expanded cases. The reduction of the peak vorticity is much higher for the under-expanded case as compared to the ideal case, consistent with the unsteady pressure measurements discussed earlier, where control is more effective for under-expanded jets. Given the fact that microjets thicken the initial shear layer, the lower peak vorticity value signifies a shear layer with lower velocity gradients which leads to the generation of weaker azimuthal vortices with microjet control. Consequently, the upstream propagating acoustic waves are weaker due to the less violent interaction between the diminished vortices and the ground. This sequence of events can eventually lead to the significantly weakening of the feedback loop and the subsequent reduction in the overall unsteadiness of the supersonic impinging jet flow.

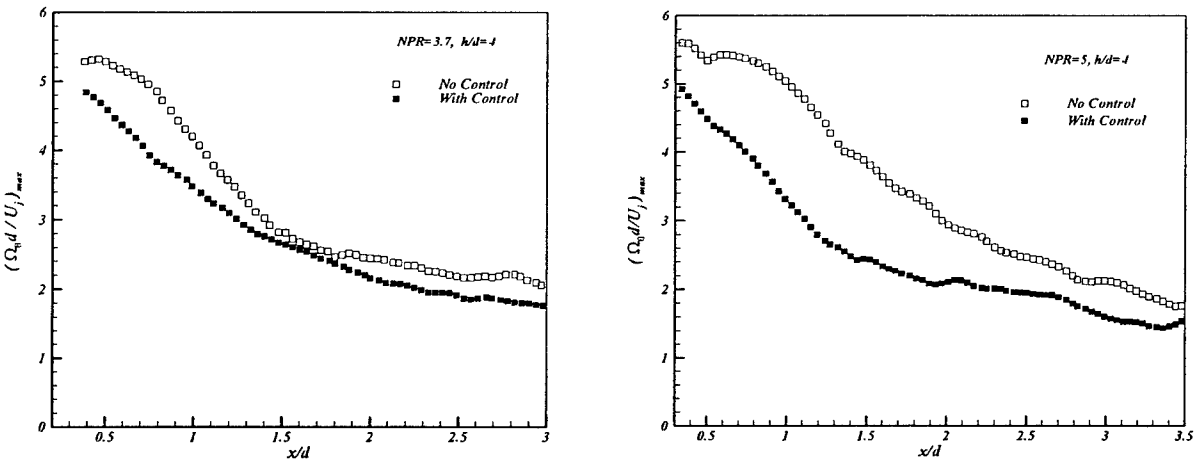

Fig. 20 - Axial variation of peak, normalized, azimuthal vorticity for NPR=3.7and NPR=5

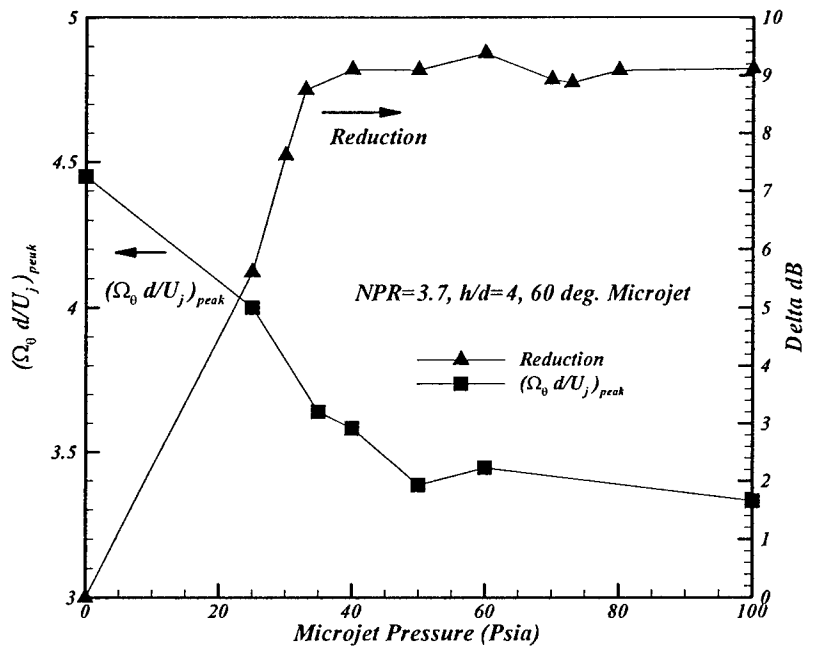

Fig. 21 - Effect of microjet operating pressure on the strength of azimuthal vorticity NPR=3.7, h/d=4, 60° microjets

Similar to Fig. 19 it is equally interesting to see how the strength of azimuthal vorticity varies as a function of microjet operating pressure. Fig. 21 shows the variation of the peak value of the azimuthal vorticity measured at x/d=1 as a function of the microjet pressure. Clearly, the strength of azimuthal vorticity decreases as the microjet pressure increases, and similar to the trend observed in Fig. 18, this decay saturates at about the same pressure. As before, there is a direct (inverse) correlation between the peak azimuthal vorticity and the reduction of the unsteady pressure loads which again suggests that the effectiveness of microjet control is also closely related to the redistribution of the azimuthal vorticity.

4.3 The Streamwise Vorticity Field

In our earlier publications (Alvi et. al, 2003 and Lou et. al, 2006) we have hypothesized that the redirection of the azimuthal vorticity into the streamwise direction by microjets could weaken the primary instability structures in shear layer, thus achieving effective flow control. This was partially based on the presence of streamwise streaks observed in the shadowgraphs (Fig.7) and their marked similarity to the streaks observed in other studies (Samimy et al. 1993 and Krothapalli et al. 1998). Prompted by the visual evidence, a more quantitative examination of the role of microjets on the impinging jet flow was conducted by using stereoscopic PIV where measurements at selected cross planes of the jet flowfield were obtained. Unless specified, the stereoscopic PIV results discussed here were obtained when the microjets were set an angle of 60° and operated at 100 psia.

The cross-plane mean velocity fields measured at three different downstream locations (x/d=1.0, 1.5, and 2.0) and shown in Fig. 22, capture the three-dimensional features of the jet evolution. With the activation of microjets, Fig. 22b, the shear layer displays a strongly modulated or 'corrugated' ring with a total of 16 indentations where the azimuthal locations of

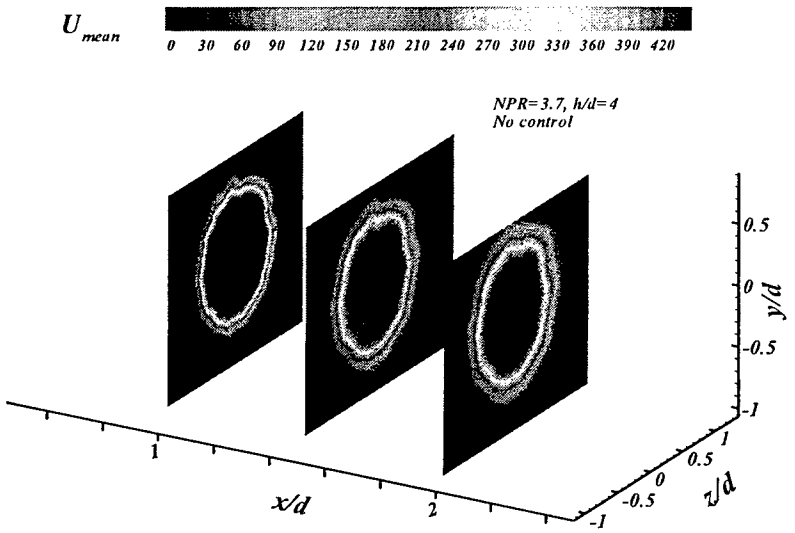

a) No Control

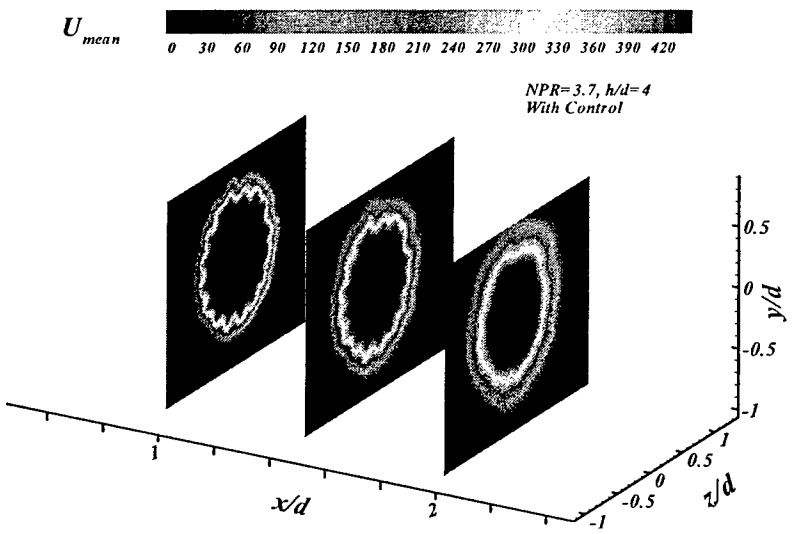

b) With Control

Fig. 22 Mean axial velocity distribution at several streamwise locations, NPR=3.7, h/d=4
(a) No Control, (b) With Control

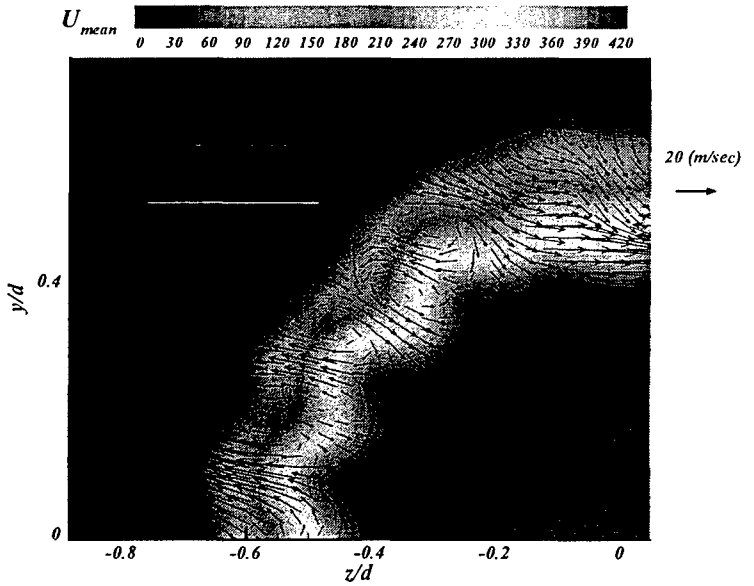

Fig. 23 Detail of the velocity field in the cross section, NPR=3.7, h/d=4

these indentations correspond to the microjet positions around the nozzle periphery. As proceeds downstream, the shear layer grows and the indentations become more diffused and eventually become difficult to identify x/d=2.0.

A close-up examination of the velocity field distribution with flow control at the x/d=1 cross plane, shown in Fig. 23, reveals that very high induction velocities exist around these mincrojet-induced indentations. For the sake of clarity, only the velocity distribution in the upper-left quarter of the jet is shown here. The in-plane velocity vectors are superimposed on the color contours of the out-of-plane component, i.e. the streamwise or axial velocity. The velocity vectors clearly show that around theses corrugated structures, the core jet flow expands outward on the lobes or the peaks of the structures while ambient flows are entrained inward in the trough regions. This significantly enhances the local mixing rate in the shear layer, thus increasing the shear layer thickness, a behavior which is consistent with the measurements of the shear layer thickness discussed earlier. These cross-stream measurements also indicate that the

generation of streamwise vortices due to microjets promotes a stronger three-dimensionality in the flow.

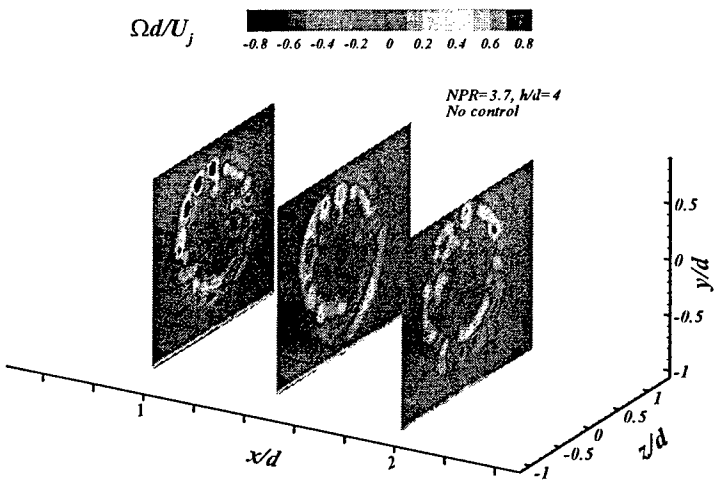

a) No Control

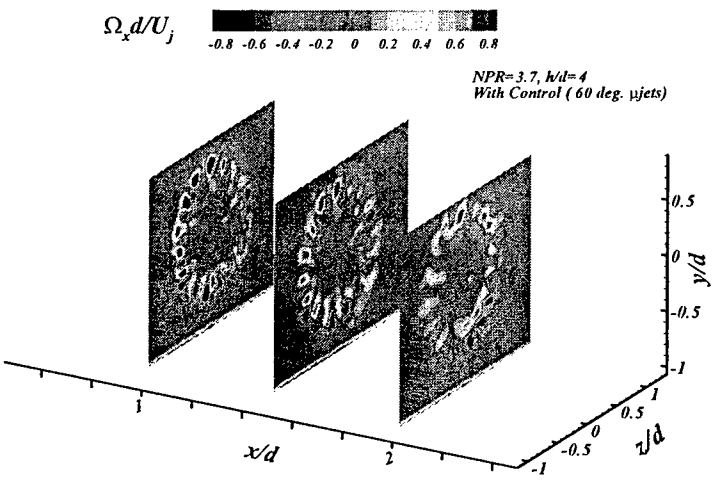

b) With Control

Fig. 24 - Ensemble-averaged streamwise vorticity distribution at the cross planes of the jet flow, NPR=3.7, h/d=4

Fig. 24 shows the *ensemble averaged* streamwise vorticity distributions at different cross planes, with and without microjet control, respectively. A comparison of the no-control case, Fig. 24a, to the microjet control data, Fig. 24b, clearly shows that the activation of microjets introduces a higher level of coherent streamwise vorticity in the jet shear layer. As it evolves downstream, the coherent (streamwise) vortical structures, become more diffused, similar to the behavior observed in Fig. 21b. However, the streamwise vorticity is still significantly higher and more organized. Compared to the no-control case of Fig. 23a, there is no evidence that these vortices have gone through pairing or merging process as have been observed in some low-speed experiments. The decrease level of vorticity at x/d=2 indicates that these structures have lost some of their coherence as they propagate downstream and interact with the primary instability waves and the flow turbulence.

In order to provide a more quantitative measure of the streamwise vorticity with and without control, in Fig. 25 we plot the strength of streamwise vorticity at a radial position corresponding to the center of the shear layer of the primary jet. This is done for two downstream locations, x/d = 1 and 2, respectively. Only one quarter of the vorticity distribution in the jet periphery is shown as it is representative of the entire axisymmetric flowfield. Each of the organized, counter-rotating vorticity pair due to microjet control can be identified here as an adjacent pair of a large-amplitude, vorticity peak (counter-clockwise vorticity) followed by a valley (clockwise). As expected, a total of four vorticity peak-and-valley pairs are clearly observed in one quadrant (filled symbols), where their locations roughly correspond to the points at which the microjets interact with the jet shear layer. In comparison, the vorticity distribution for the no control case (open symbols) has a significantly lower level and is not well-organized. At x/d=1, the maximum normalized peak vorticity value with control is of the order of 1 is

substantial (about 25%) relative to the maximum azimuthal shear layer vorticity (of the order of 4 without control, Fig. 20). The redirection of this considerable amount of the azimuthal vorticity into the streamwise direction certainly plays a vital role in weakening the primary flow stability and the subsequent reduction of the overall flow unsteadiness. Further downstream (x/d=2), although the vorticity level of the streamwise vortices declines slightly but they still maintain rather coherent alignment as shown in Fig. 25b.

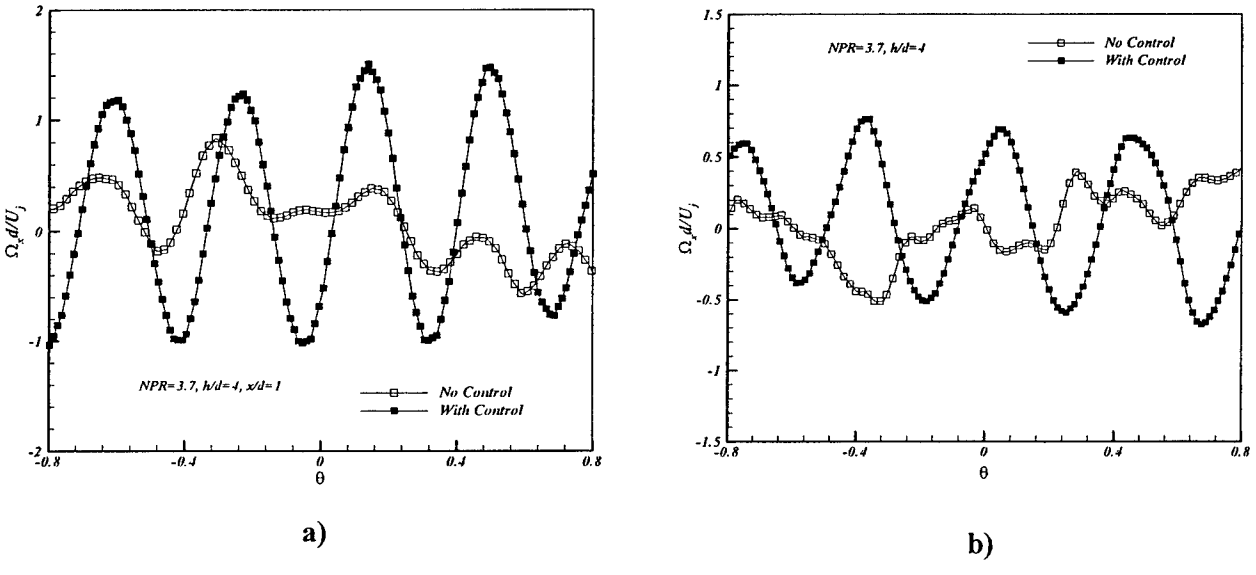

a) b)

Fig. 25 - *Ensemble-averaged* streamwise vorticity distribution along the azimuthal direction, NPR=3.7, h/d=4, (a)x/d=1; (b)x/d=2

4.4 A Discussion of the Physical Mechanisms behind Microjet Control

The results discussed in prior sections clearly demonstrate that the microjets introduce substantial streamwise vorticity which influences the development of the primary jet. Here we closely examine the underlying physical mechanism(s) behind microjet control. Only a brief discussion is presented here, more details can be found in Lou et al. (2006, JFM, to be submitted) The first question one may ask is: "what is the source of vorticity for these streamwise vortices?"

There are at least three potential sources of vorticity: (1) redirected from the primary azimuthal vorticity, (2) supplied by the microjet vorticity, or (3) generated due to the misalignment between the density and pressure fields as a result of microjet control. In order to understand the origin of the vortical structures and to determine the source of vorticity, the time-averaged vorticity transport equation, appropriate for the present flow configuration, is considered:

$$\frac{D\bar{\Omega}}{Dt} = \bar{\Omega} \cdot \nabla \bar{U} - \nabla \frac{1}{\rho} \times \nabla p + \upsilon \nabla^2 \bar{\Omega} \qquad (1)$$

where $\bar{\Omega}$, $\bar{U}$, ρ, p represent the vorticity, the velocity, the density and the pressure, respectively. This equation shows that the existing vorticity field can be convected, stretched, distorted and diffused. In particular, the second term on the right side which represents the baroclinic torque generation term, usually emerges when the pressure and density gradient is misaligned; this could be a very strong source of vorticity generation in very high-speed flows (Marble et al 1990, and Waitz et al 1992). However, as pointed by Kim & Samimy (1999), the effect of streamwise vortices generated by the baroclinic torque on an axisymmetric flow is usually negligible.

Although equation 1 does not have other explicit source terms, new circulation can enter a flow through imposed initial conditions and/or boundary conditions. In the present study, one potential source for the streamwise vorticity is the vorticity contained in the microjet streams. Based on an order of magnitude analysis, it can be easily shown that the collective circulation from all microjets is less than 10% of the circulation of streamwise vorticity measured in the primary jet when the microjets are turned on. This suggests that a significant portion of the streamwise vorticity will have to come from the existing vorticity by other processes, namely: stretching or tilting of the azimuthal vorticity.

To illustrate this further, the evolution of the streamwise vorticity component (Ω_x) can be described using the following equation if both the baroclinic and the diffusion terms are neglected:

$$\frac{D\Omega_x}{Dt} = \Omega_x \frac{\partial U}{\partial x} + \Omega_\theta \frac{1}{r}\frac{\partial U}{\partial \theta} + \Omega_r \frac{\partial U}{\partial r} \qquad (2)$$

Here the first term on the right hand side represents the stretching of the existing streamwise vorticity under streamwise velocity gradient. This term is important if the flow is accelerating locally as it is the case for the flow near the nozzle exit of an under-expanded jet. The second and third terms represent the tilting of the azimuthal and radial vorticity, respectively, into the streamwise direction. For an axisymmetric jet without control, these two terms are nearly equal to zero. In order to redistribute the vorticity, it is clear that microjets control must either cause higher jet axial velocity gradient along azimuthal direction, $\frac{\partial U}{r\partial \theta}$, and/or generate significant radial vorticity, Ω_r (since there is already a strong velocity gradient across the shear layer, $\frac{\partial U}{\partial r}$).

Fig. 26a shows the azimuthal distributions of the mean axial velocity, U , and streamwise vorticity at a radius of r/d=0.55. For an axisymmetric jet without control, the mean axial velocity, U , distribution along the azimuthal direction should be nominally constant. However, microjet control significantly changes the mean axial velocity distribution, shown in Fig. 26a. A distinct wavy pattern consisting of four modulations can be clearly identified when the microjets are on. It is to be noted that this wavy pattern is not a transient phenomenon since it persists through an ensemble average of 400 instantaneous PIV realizations.

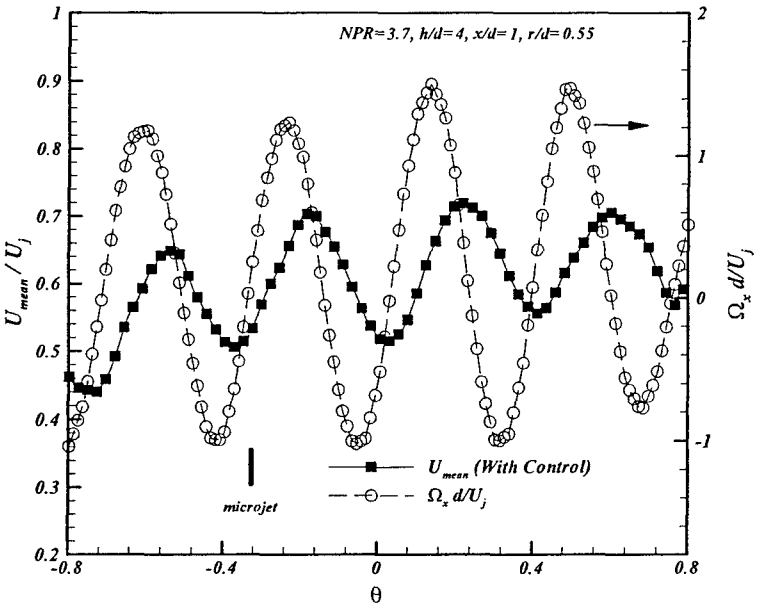

a) Distribution of axial velocity and streamwise vorticity

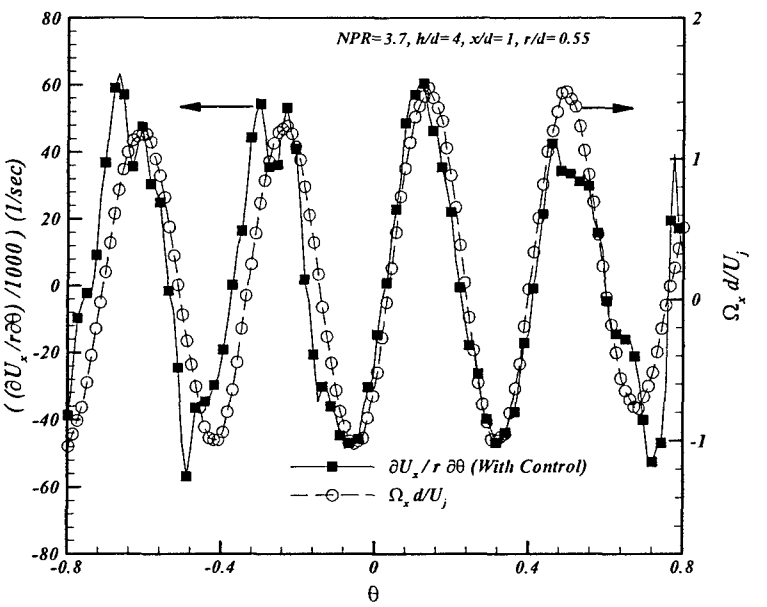

b) Correlation between $\partial U_x/r\partial\theta$ and $\Omega_x d/U_j$

Fig. 26 Mean axial velocity and streamwise vorticity distribution along the azimuthal direction at cross plane of x/d=1, NPR=3.7, h/d=4

The corresponding azimuthal location of a representative microjet is marked by the solid vertical line near the lower part of the graph. It can be seen that the microjet is roughly co-located at the minima of the mean axial velocity distribution, suggesting that the presence of microjet streams essentially slow down the main jet flow locally. This is consistent with the flow behavior expected from a jet in a cross flow. In order to maintain a constant momentum, the neighboring regions around the microjet streams have to accelerate. This local minima and maxima result in a higher axial velocity gradient, $\frac{\partial U}{r\partial\theta}$, along the azimuthal direction for the control case. This gradient is included in the second term on the right side of equation (2), thus contributing to the redirection of the azimuthal vorticity into streamwise vorticity. Fig. 22a shows a clear correlation between the azimuthal mean axial velocity gradient, $\frac{\partial U}{\partial\theta}$, and the presence of the streamwise vorticity for the microjets control case. Fig. 26b plots the mean axial velocity gradient, $\frac{\partial U}{r\partial\theta}$, distribution along the azimuthal direction as along with the streamwise vorticity. The remarkable match between these two terms provides strong evidence about the direct role played by the mean axial velocity gradient, $\frac{\partial U}{r\partial\theta}$ in generating streamwise vorticity.

Similarly, one can also examine the contribution from the third term in the vorticity transportation equation (2), $\Omega_r \frac{\partial U}{\partial r}$. It is well known that there is a strong axial velocity gradient, $\frac{\partial U}{\partial r}$, across the jet shear layer. However, the axisymmetric jet shear layer does not have a substantial radial vorticity component Ω_r without microjet control. However, by examining the vorticity equation along the radial direction it can be shown that a significant amount of the radial vorticity component can be generated by redirection of the azimuthal

component. This radial vorticity can then be tilted into the streamwise direction by the presence of a steep velocity gradient, $\frac{\partial U}{\partial r}$, in the jet shear layer as seen in equation 2.

In summary, the PIV measurements reveal that the activation of the microjets introduces strong and well-organized streamwise vorticity in the jet shear layer. This increase is concomitant with a decrease in the azimuthal vorticity. The combined effect of an increase in shear layer thickness and a decrease of the peak azimuthal vorticity efficiently suppresses the primary shear layer instability, thus attenuates the large-scale structures and upstream propagating acoustic waves. This reduction of azimuthal vorticity is believed to be the direct result of vorticity being redirected into the streamwise direction through the tilting and stretching process. Detailed 3D PIV measurement in the jet cross planes reveal a clearly correlation between the azimuthal gradient of mean axial and radial velocity and the presence of the streamwise vorticity for the microjet control case, further confirming the role of the former in generating the latter. The emergence of three dimensionality due to the streamwise vorticity further disrupt the spatial coherent of the coupling between the acoustic wave and shear layer instability. This sequence of events leads to the weakening of the feedback loop, and the subsequent reduction of the overall unsteadiness of the supersonic impinging jet flow.

5. ACTIVE CLOSED-LOOP CONTROL OF IMPINGEMENT TONES

The motivation for considering active control comes from the behavior of the flow-field in the presence of the supersonic microjets. As can be seen in Figs. 8-10, microjets disrupt the feedback loop thereby reducing the OASPL. Not only is the reduction unpredictable but it also varies for the same nominal conditions (see Choi et al., 2005). We therefore examine the use of closed-loop control that uses on-line measurements and active-adaptive algorithms.

5.1 A Reduced-Order Model of Impingement Tones

Much of feedback control consists of designing suitable external actuators that introduce a control input so as to alter, typically, the dynamic characteristics of the process being controlled. In many of these problems, the control method begins with a description of the process in the form of a differential equation

$$\dot{x} = f(x,u)$$

where x denotes the process state, and u denotes the control input-source. The control strategy then consists of determining a feedback signal according to the rule

$$u = g(x)$$

where $g(.)$ is to be determined so as to realize the desired objective in the process.

The reduced-order model adopted for the control of impingement tones is based on the vortex-sheet jet model of Tam (1990). Within a short distance ($\sim 0.01R_j$) downstream from the nozzle exit, the jet can be idealized as a uniform stream of velocity U_j and radius R_j bounded by a vortex sheet. Small-amplitude disturbances are superimposed on the vortex sheet (see Fig. 27). By starting from the linearized equation of motion of a compressible flow, it can be shown that the governing equations for the problem are:

$$\frac{1}{a_\infty^2}\frac{\partial^2 p_+}{\partial t^2} = \nabla^2 p_+ \qquad (r \in \Omega_2)$$

$$\frac{1}{a_j^2}\left(\frac{\partial}{\partial t}+U_j\frac{\partial}{\partial z}\right)^2 p_- = \nabla^2 p_- \qquad (r\in\Omega_1) \tag{3}$$

where $p_+(r,\theta,t)$ and $p_-(r,\theta,t)$ be the pressures associated with the disturbances outside and inside the jet, denoted respectively by domains Ω_2 and Ω_1 where Ω_1 denotes jet-core which extends from z = -∞ to z = +∞, Ω_2 denotes the domain outside the jet-core and (r,θ,t) are the cylindrical coordinates, a_∞ and a_j are the speed of sound outside and inside the jet and U_j is the main jet speed. The aim here is to choose u, the microjet velocity such that the pressure p is reduced in magnitude. In order to extract as much information possible about the state of the system, we adopt the Principal Decomposition Method (POD). The Proper Orthogonal Decomposition (POD) is a tool used to systematically extract the most energetic modes from a set of realizations from the underlying system.

By separation of variables, we can write for the outer area Ω_2

$$p_+(r,\theta,z,t)=\sum_{i=1}^{L} X_i(t)\Phi_i(r,\theta,z) \tag{4}$$

where X_i is the state variable, and $\{\Phi_i\}$ are the POD modes. Using the wave equation, the equality conditions, the effect of the microjets, and the flow condition on the lift plate, we can obtain a model of the form

$$\ddot{X}_j(t)=a_\infty^2\sum_{i=1}^{L}\left(\nabla^2\Phi_i,\Phi_j\right)X_i(t) \qquad\qquad j=1,\ldots,L \tag{5}$$

where $\{\Phi_i\}$ is a function of microjet velocity. Eq. (5) will be suitably used for future control designs. The POD modes can be obtained as the solution of an optimization problem

$$\underset{\Psi}{Min}\, J_m(\bar{\phi}_1,\ldots,\bar{\phi}_l)=\sum_{j=1}^{m}\left\| Y_j-\sum_{k=1}^{l}\left(Y_j^T\bar{\phi}_k\right)\bar{\phi}_k \right\|^2 \tag{6}$$

subjected to: $\bar{\phi}_i^T\bar{\phi}_j=\delta_{i,j},\ 1\le i,j\le l,\ \Psi=\left[\bar{\phi}_1,\ldots,\bar{\phi}_l\right]$

where $Y_j \in \Re^n$ is the vector of flow data F at time $t = t_j$ (see Holmes et al., 1996 for further details).

It can be seen from Equation (4) that in order to find the POD modes of the system, the calculation of pressure at all flow points is needed. This is not feasible either experimentally or computationally due to obvious constraints. However, our main goal is to model the impingement tones and it is worth noting that the key ingredients that contribute to their formation such as the initiation of the shear layer instability waves and their interaction with the acoustic waves appear to be localized at the jet nozzle. Therefore, we derive the impingement tones model by focusing only on the POD of the pressure field close to the nozzle. That is, we derive the control strategy using the expansion:

$$p_+(r = R_s, \theta, z = z_{nozzle}, t) \equiv p(\theta, t) = \sum_{i=1}^{I} T_i(t)\phi_i(\theta) \tag{7}$$

where R_s is the radial position of the sensors on the lift plate. Note that ϕ_i's in Equation (7) are, quite likely, a subset of Φ_i's in Equation (4) which are the modes of the entire flow field. The state space equation corresponding to these reduced set of modes are given by:

$$\ddot{T}_j(t) = a_\infty^2 \sum_{i=1}^{L} \left(\nabla^2 \phi_i, \phi_j\right) T_i(t) \qquad j = 1, \ldots, L \tag{8}$$

with the inner product suitably defined. In vector form, this becomes:

$$\dot{T}(t) = \breve{A}(p_\mu) T(t) \tag{9}$$

Once the mode shapes are determined, we simply choose the control strategy as:

$$p_\mu(\theta) = k\phi_1(\theta) \tag{10}$$

where ϕ_1 is the most energetic mode in Equation (7) and k is a calibration gain. The complete closed-loop procedure therefore consists of collecting pressure measurements $p(\theta, t)$, expanding them using POD modes as in Equation (7), determining the dominant mode ϕ_1, and matching the control input - which is the microjet pressure distribution along the nozzle - to this dominant mode as in Equation (10).

The closed-loop control approach used here is distinctly different from the traditional feedback control paradigm where the control input is typically required to be modulated at the natural frequencies of the system. The latter, in turn, mandates that the external actuator have the necessary bandwidth for operating at the natural frequencies. In the problem under consideration, the edge tones associated with the flow-field are typically a few kilohertz. Given the current valve technology, modulating the microjets at the system frequencies is a near impossibility. The approach presented above overcomes this hurdle by modulating the control input, u, at a slow time-scale, so that it behaves like a parameter. If this control input is chosen judiciously, then even small and slow changes in this "parameter" can lead to large changes in the process dynamics, as is shown below.

5.2 Experimental Results

The closed-loop control strategy described above was implemented at the STOVL supersonic jet facility of the Fluid Mechanics Research Laboratory, shown in Fig. 4. As discussed earlier, four banks of microjets were distributed around the nozzle exit, while pressure fluctuations were sensed using six Kulite^{TM} transducers placed symmetrically around the nozzle periphery plate, at r/d = 1.3, from the nozzle centerline where d is the nozzle throat diameter. The control experiment was performed for a range of heights (of the nozzle above ground).

At each height, in addition to the mode-matched control, active control was also implemented by supplying all the microjets with a uniform pressure, the results of this uniform forcing have already been described in §3 and §4. The latter case, where the spatial distribution of microjet pressure around the nozzle exit was kept uniform, can be viewed as an open-loop control procedure. To ensure a fair comparison between the two control methods, the main nozzle was forced to operate under constant condition throughout the whole process. The calibration constant k in Equation (8) was chosen such that the minimum and maximum values of the POD mode over θ correspond to 70psi and 120psi, respectively, which ensured maximum effectiveness of the actuator. Fig. 28 (a) shows the shape of the first mode and the suggested microjet bank pressure distribution for several heights and 28(b) shows a block diagram of the active closed-loop control method. Fig. 29 shows the results for the closed loop control strategy, which indicates better performance throughout all operational conditions, with a large

improvement at heights h/d = 4, 4.5 and 5. The reason for this increased pressure reduction can be attributed to the percentage of energy contained in the dominant mode, which is used in the control strategy. Seen in Table 1, at heights 4 to 5, the energy content of the first mode is above 90 %. In contrast, at heights 2 and 3, the energy level drops to about 50 % and hence the corresponding improvement in the closed-loop strategy also drops to about half the db-value at heights 2 and 3 compared to at heights 4 and 5. It was observed that for a different configuration where the microjets were at a 30-degree inclination, the same mode-matched strategy resulted in a mostly comparable, and at times slightly improved, performance compared to steady-microjet injection (see Fig. 30).

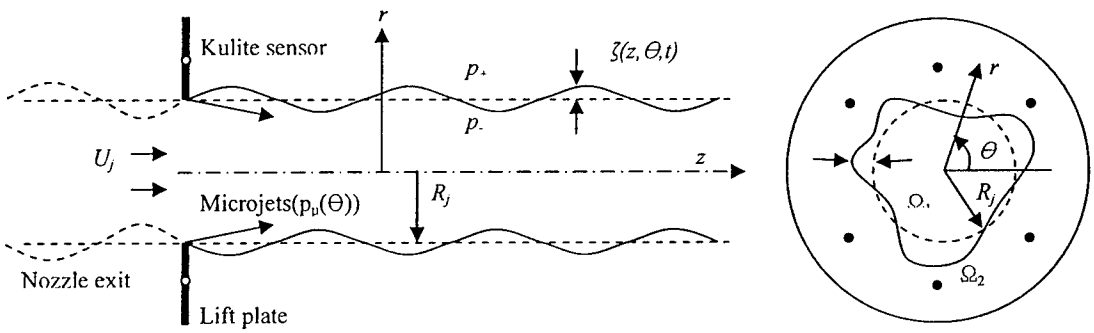

Fig. 27 - Vortex-sheet jet model for the impingement tones control problem. Location of microjets and pressure sensors are also shown

Table 1 The energy content of the first four modes at each height (NPR=3.7, 20◦ injection)

h/d	Mode 1	Mode 2	Mode 3	Mode 4
2.0	0.4615	0.2488	0.1785	0.1111
3.0	0.5515	0.2745	0.1144	0.0597
4.0	0.8609	0.0691	0.0443	0.0257
4.5	0.8836	0.0517	0.0389	0.0258
5.0	0.8736	0.0757	0.0314	0.0194

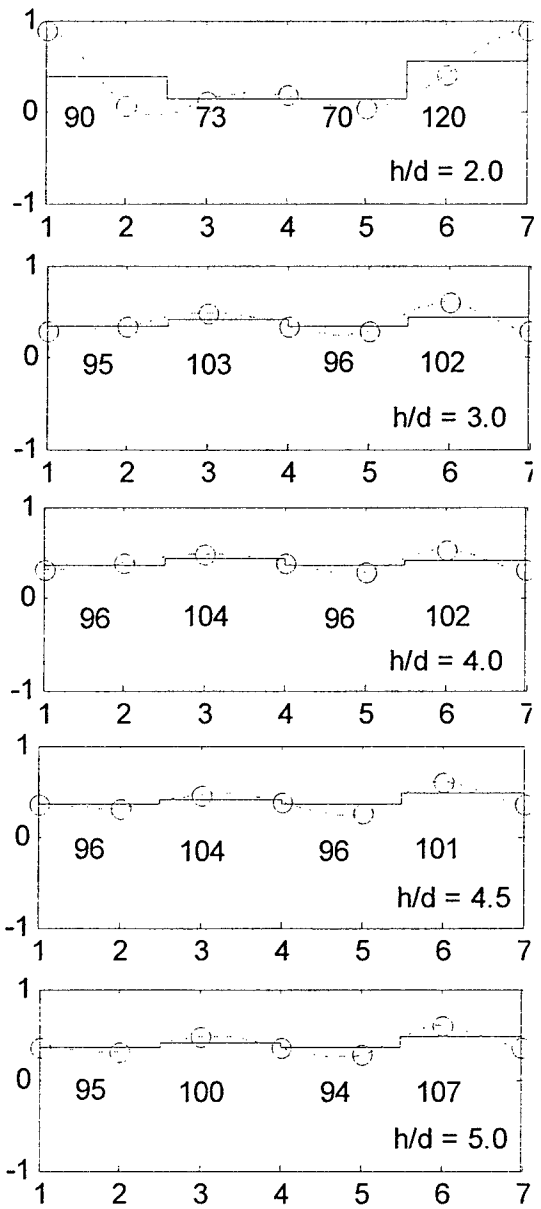

(a)

Figure 28 - (a) The first mode shape and suggested microjet pressure distribution for each height. h is the height of the lift-plate from ground and D is the diameter of the lift-plate

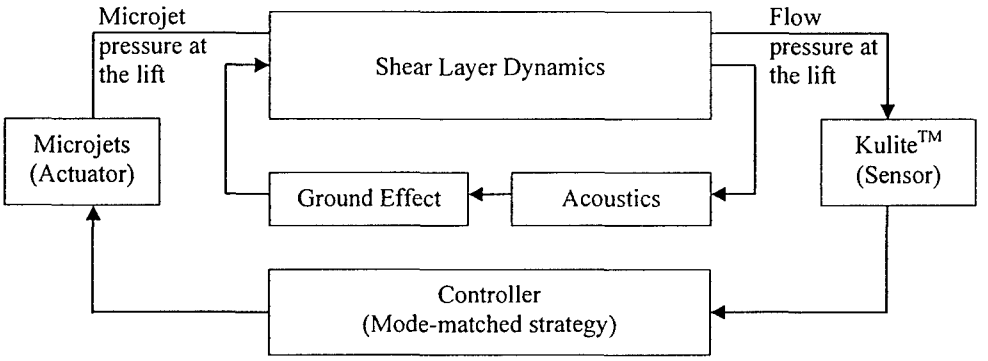

(b)

Fig. 28 - (b) Block diagram of the closed-loop control program of impingement tones.

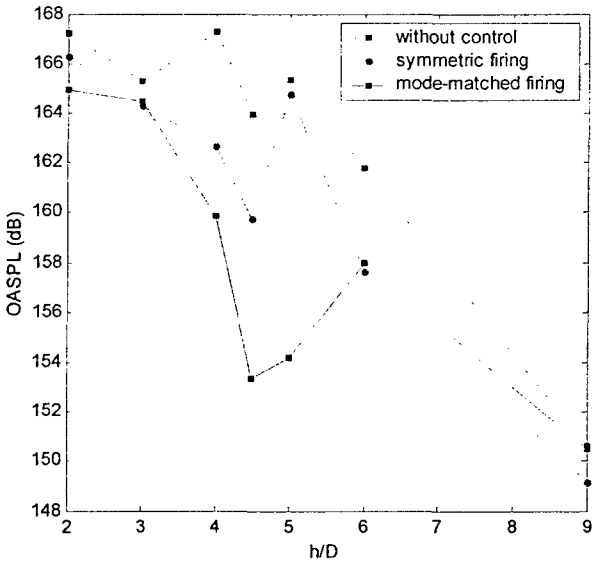

Fig. 29- Overall sound pressure levels (OASPL) for different control (NPR=3.7) 20° microjet inclination

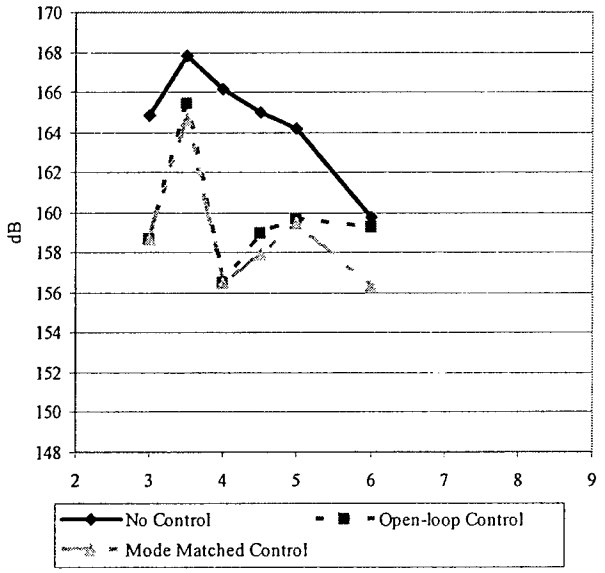

Fig. 30- Overall sound pressure levels (OASPL) for different control (NPR=3.7), 30° microjet inclination

6. ACTIVE CONTROL OF IMPINGEMENT TONES USING MODULATED MICROJETS

To obtain a uniform and guaranteed reduction of the OASPL at all operating conditions, a closed-loop control based on POD was conducted. As shown in the previous section, it was observed that the performance of POD based control was still sensitive to changes in the operating conditions, and in particular, to the distance between nozzle exit and the impinging region. To obtain a more consistent noise reduction over a larger range of jet operating conditions, we examined a different control strategy, which consists of a technique that *pulses* the microjet flow. The rationale for introducing pulsing is discussed below.

For a given mass flow rate $\dot{m} = \rho A U_{\mu.0}$, the force induced by steady microjet injection is given by the rate of momentum change in time. Using the same mass flow rate, an unsteady injection can exert more force on the primary jet shear layer of the flow than steady injection, in an average sense. Equation (11) described below shows that, if as an example, the unsteady flow through the microjets is represented in sinusoidal form, the additional force increase is realized by $\rho A\left(B^2/2\right)$:

$$F_{\mu.steady} = \dot{m} U_{\mu.0} = \rho A U_{\mu.0}^2$$

$$U_{\mu.steady} = U_{\mu.0} + B\sin(\omega t)$$

$$F_{\mu.}(t) = \dot{m} U_{\mu.unsteady} = \rho A\left(U_{\mu.0} + B\sin(\omega t)\right)^2$$

$$\dot{F}_{\mu.steady} = \dot{m} U_{\mu.0} = \rho A U_{\mu.0}^2$$

$$\overline{F_{\mu.}(t)} = \frac{\omega}{2\pi}\int_0^{2\pi/\omega} \dot{m} U_{\mu.unsteady}\, dt = \rho A\left(U_{\mu.0}^2 + \frac{B^2}{2}\right) \qquad (11)$$

That is, for a given mass flow rate, a pulsed injection can generate more momentum than steady continuous microjet injection, and hence can perhaps have a stronger impact on the jet shear layer, thus disrupting the feedback mechanism more effectively and hence reducing the noise more significantly.

6.1 Development of Modulated Microjets for Optimal Control

Rotating Cap Valve

A cap with 16 teeth as shown in Fig. 31 was designed to enable pulsing of the microjets. While rotating, the circumferentially located teeth cut the microjet stream periodically thereby generating a pulsing microjet injection. A preliminary small-scale experiment was carried out using this rotating cap, the results of which are shown in Fig. 32. This figure shows the total pressure signal measured by a Kulite transducer near the microjet exit. It clearly illustrates that the pulsing action can be sustained up to a few hundred Hz while maintaining significant momentum in the microjets. More details of this design can be found in Choi et al. (2005a).

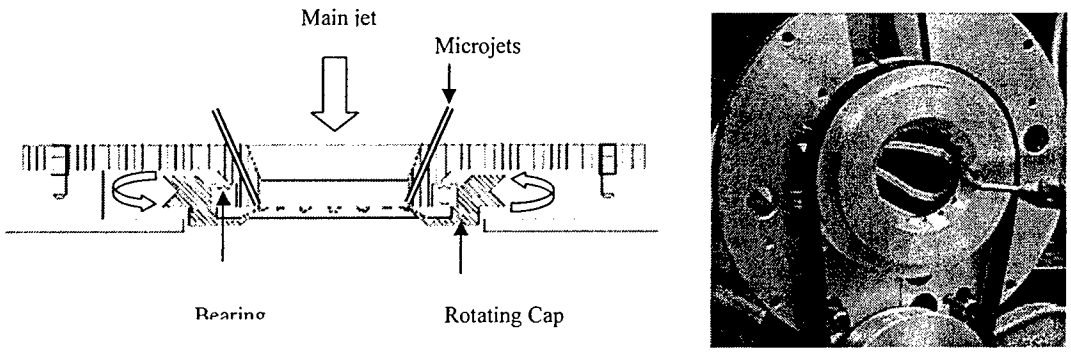

(a) (b)

Fig. 31 - (a) Schematic diagram of rotating cap, (b) picture of rotating cap

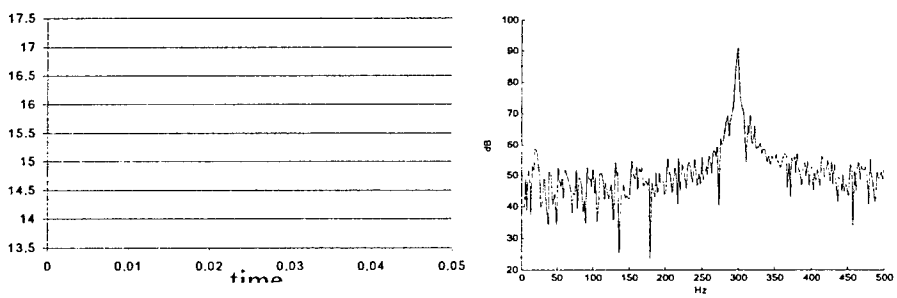

(a) **(b)**

Fig. 32 - **(a)** Time history of pressure at the microjet exit (b) Spectra of the pressure signal

6.2 Effectiveness of Modulated Microjets

Representative results obtained using the collocated rotating cap for impingement control are shown in Fig. 33. In this figure, the pulsed jet results obtained are compared to the steady microjet injection case. The noise level is measured by the microphone located at 25 cm away from the nozzle axis because it was observed that the Kulite transducer mounted on the lift plate does not capture the correct signal due to the vibration of the motor.

For steady and pulsed injections, the supply pressure to the microjets was set to 100 psig. Under the same supply pressure, the peak value of flow modulation due to pulsing roughly corresponds to the flow exit speed during steady injection, and hence the duty cycle of pulsing determines the relative mass flow rate due to pulsing as compared to the steady injection case. Here the resultant pulsing speed of the rotating cap was set to 121 Hz, which is a moderate speed and does not lead to a broadband noise increase. Fig. 33 (b) illustrates that pulsing of microjets using the collocated rotating cap (green line) reduces noise to levels that are comparable to the steady injection case (red line). Furthermore pulsed injection appears to work significantly better for cases at which steady injection is not very effective, such as at h/d=3.5. This combined with the fact that this noise reduction is achieved with less than 75% of the steady injection mass flow rate, makes pulsed injection very attractive. Experiments in Fig. 33(a) conducted using a 42% duty cycle pulsed jets, show that significant noise reduction, comparable to the steady microjets, can be achieved with less than 50% of steady microjet flow rate.

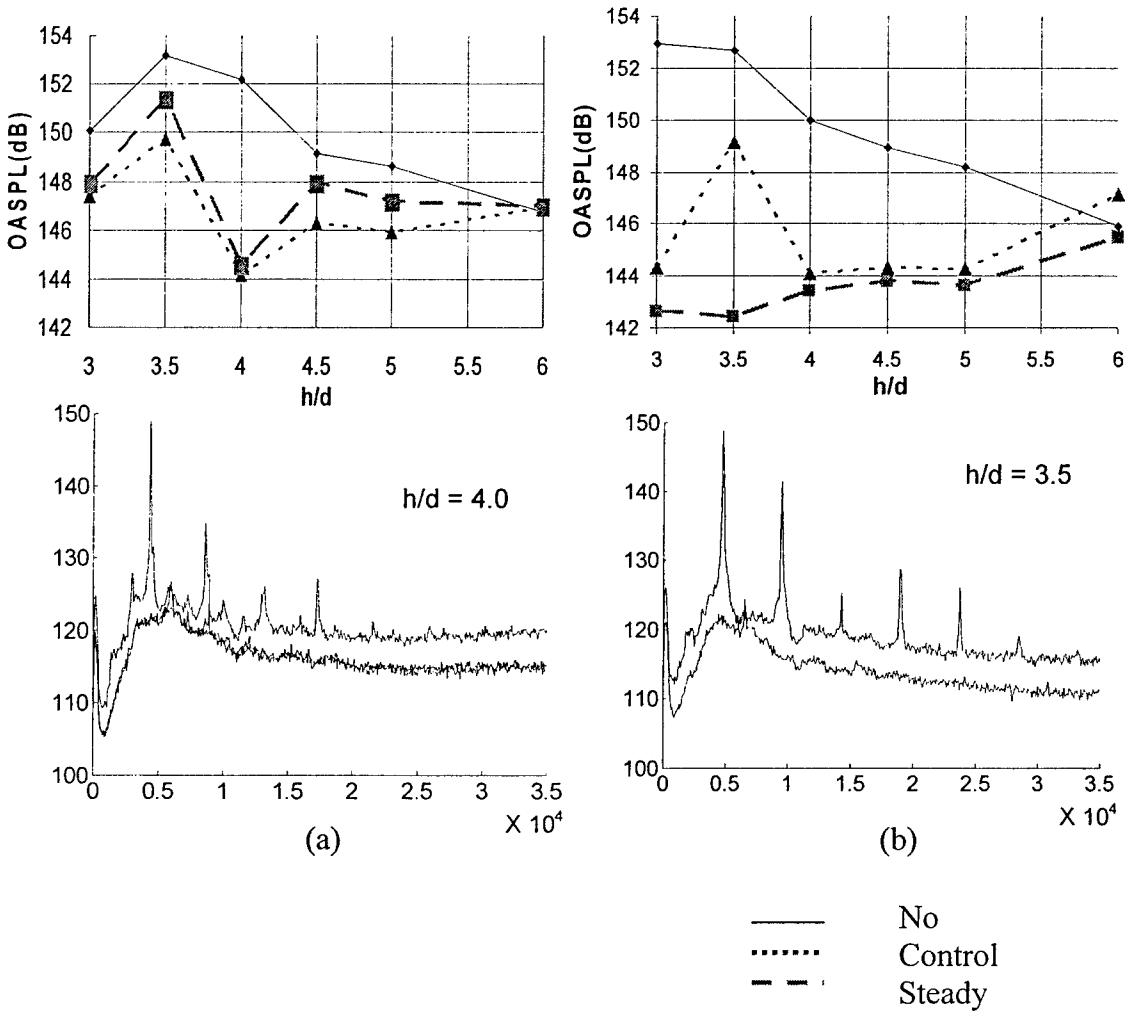

Fig- 33 Experimental result (a) Case of d_c = 42% (b) Case of d_c = 74%

6.3 Control Parameters

In order to further understand the impact of the rotating cap and the sensitivity of the impinging flow field to the pulsing parameters such as frequency and duty-cycle, a number of parametric studies were conducted, which are summarized below:

(a) Effect of duty-cycle (d_c):

For example, if d_c is the duty cycle of pulsing, which is the ratio of the valve opening time to pulsing period, then

$$d_c = 100\left(\frac{N_h d_h}{\pi d}\right)(\%) \tag{12}$$

where d is the main jet diameter, d_h is the diameter of the holes in the rotating cap (see Fig. 34), and N_h is the number of holes in the rotating cap. This implies that the duty cycle (d_c) is changed by varying the number and diameter of holes of the rotating cap.

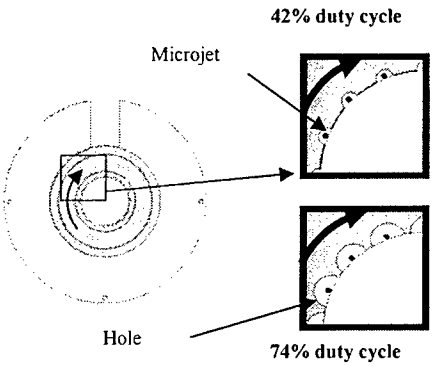

Fig. 34 - Modification of duty cycle by changing hole size

Two points should be noted from the Fig. 33. The first is that both pulsing and steady microjet action yield about the same amount of pressure reduction, and since the supply pressures were the same, it implies that the pulsing action allows noise reduction to occur at 42% of the mass flow rate needed for the steady case. The second is that a significantly larger reduction can be obtained from the pulsing action under certain duty cycles, which follows from Fig. 33 b). It was in fact observed that the pulsed injection completely destroyed the distinct impinging tones at almost all *h/d*.

(b) Effect of frequency (f_{pulse}): One revolution of the cap introduces 16 pulses since the cap has 16 internal holes. Moreover, the pulley which drives the rotating cap has a smaller diameter than the rotating cap. Hence, the pulsing speed is obtained from the following relations:

$$f_{pulse} = 16 \times \left(D_{pulley} / D_{cap}\right) RPM_{pulley} / 60 \tag{13}$$

where D_{cap} = 2.625 in, D_{pulley} = 2 in. Here the resultant pulsing speed by the rotating cap was set

to 121 Hz, which corresponds to a moderate motor speed of 596 rpm. The rotating cap was spun over a range of frequencies from 0 to 300 Hz. The corresponding results show that over this range, the amount of noise reduction is quite independent of f_{pulse}.

(c) Effect of phase-difference ϕ_{phase}:

If the number of holes in the rotating cap is the same as that of microjets, all the microjets pulse synchronously. To achieve a phase difference between two adjacent microjet pulses, the number of holes in the cap was chosen to be different from that of microjets. This phase difference, ϕ_{phase}, can be calculated using equation (14)

$$\phi_{phase} = \left(\frac{N_h}{N_m} - 1 \right) \times 360 \qquad (14)$$

where N_m is the number of microjets

Two experiments were conducted by changing the rotating direction of the cap to check the effect of phase lead and phase lag on noise reduction. The results obtained for a phase = 45° and a phase = -45° are compared with the synchronously pulsed injection case, where the duty cycle was maintained at 42%. We note that these phase variations did not result in any noticeable improvement over the synchronous scheme and uneven noise reduction for various heights is still conspicuous.

7. DEVELOPMENT OF AN ACOUSTIC MODEL FOR THE IMPINGING JET

It is well-accepted that a primary link in the impinging jet feedback is the noise generated by the impingement of the large scale vortical structures which are formed by the evolution of the instability triggered by acoustic wave near the nozzle (see Alvi et al. 2003). Here, we develop a physical model of this noise generation mechanism due to the large scale vortical structures impinging on the wall by viewing it as a head-on collision of two identical vortices. This is because, while impinging on the ground, the annihilation process of the vortical structures is approximately analogous to that of two colliding vortices. This process is schematically illustrated in Fig. 35. Overall, this model has produced very encouraging results, details of which can be found in Choi et al. (2005a). As seen in Fig. 36, which shows a comparison of the model prediction to experimental data, it not only captures the dominant frequency content but also the harmonics. Secondly, similar to the experimental result, the amplitude of each peak also tends to decrease at high frequency, which was not predicted by earlier versions of this model. Third, the amplitude of the peak matches to the value obtained from experiment. However, the overall amplitude predicted is in general much less than that of experiment data, which is due to the fact that we considered only the impinging vortex as the noise generation source. We are now improving the model but incorporating more realistic boundary conditions and flow properties, based on experimental measurements.

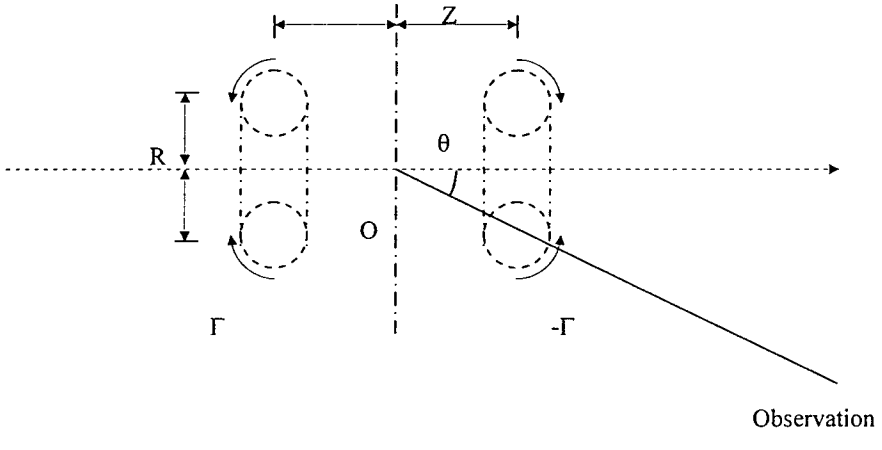

Fig. 35 - Schematic of colliding vortices; the dashed line represents the wall.

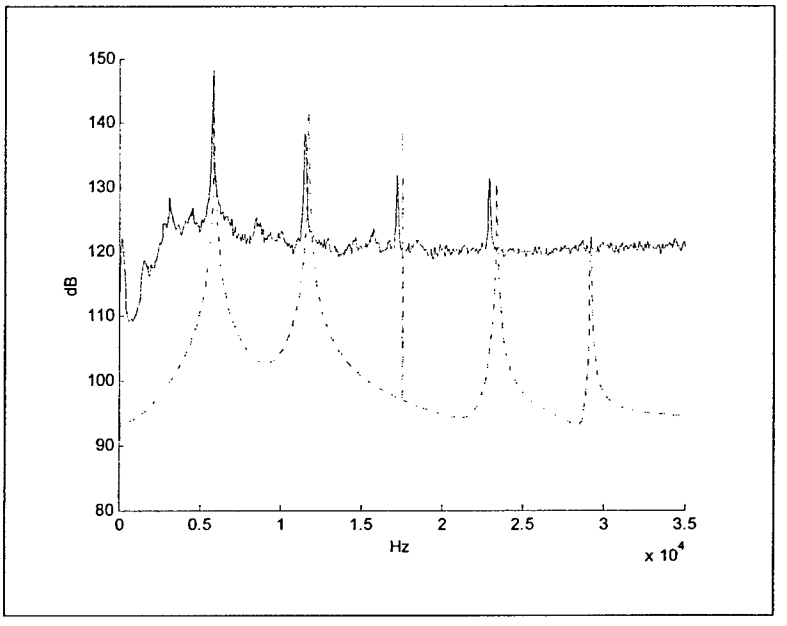

Fig. 36 - Comparison of a model prediction (dashed blue) of the impingement tones to experimental results (red).

8. CONTROL OF HOT IMPINGING JET – PRELIMINARY RESULTS

The work to-date has clearly demonstrated the potential of this approach in effectively controlling cold impinging jets, the time has come to evaluate microjet control for hot jets. This brings us closer to flow conditions that occur in practical applications while allowing us to reevaluate some of the physical mechanisms developed and proposed during the study of cold impinging jets. An upgrade to our Impinging Jet facility has just been completed which have enabled us to run the main jet(s) at temperatures between 600 and 800°F.

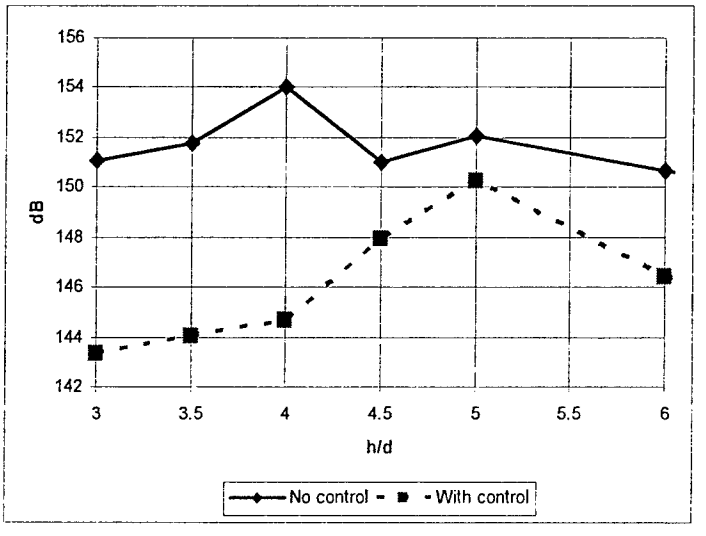

Fig. 37 - OASPL of Hot jet experiments. The steady microjet was inclined at 60° with respect to the nozzle axis. Supply pressure to microjet chamber is 100 psig. Max and min of stagnation chamber temperature are 232 F°, 201 F° respectively.

As a first step of the test using hot jet facility, we controlled the impinging tones using steady microjets. Here, the steady microjet was inclined at 60° with respect to the nozzle axis. The pressure supplied to microjet chamber was set to 100 psig. The maximum and minimum stagnation chamber temperatures were recorded to 232 F°, 201 F° respectively. As seen in Fig. 37, the microjet has proven to be an equally effective actuator for suppressing hot impinging tones too. More experiments are being planned to understand the dependency of many control parameters as we did for cold impinging jet experiment. This will be the next topic the ongoing research is expected to answer.

9. SUMMARY

In this we report we summarize the significant results of a three-year study designed to expand upon the success of using microjets for the control of supersonic impinging jets. Our aim was to better understand the physical the properties of supersonic impinging jets and develop optimal open and closed-loop control strategies in order to produce efficient control over the relevant parametric range (where the associated ground effect is an issue). Specifically, our goals were to:

a) Examine in considerable detail, the flow physics that govern this control strategy and through a better understanding of the base flowfield and the effect of microjet on its properties

b) Determine the parameters that govern the efficacy of microjet actuators. This in turn would allow one to design more effective actuators for this and similar flows.

c) investigate and develop on-line, closed-loop control strategies in order to achieve optimal flow control over the desired operating range by developing models that capture the essential flow behavior (impinging jets) and can be used to develop control algorithms

d) Explore means of providing pulsed actuation using commercially available hardware and developing pulsed actuators in-house, if needed and, finally

e) Extend the use of microjets for increasingly realistic flow conditions by implementing them in hot impinging jets.

The flowfield of impinging jets were examined in detail in this experimental study using conventional techniques such as flow visualization and acoustic measurements, as well as advanced diagnostics such as Particle Image Velocimetry. The effective of microjet control was significantly improved and as the results discussed in this report indicate, we were able to make considerable progress in all the areas described in the previous paragraph. A list of some significant outcomes resulting from this study is provided below..

- The efficacy of microjet control was significantly improved through a better understanding of the microjet parameters on control. As a result, the mass flow required for significant noise reduction, as much as 14 dB, was reduced by more than a factor of 2.
- The performance gains were achieved with minimal mass flow requirements, which was below 0.5% of the main jet mass flux for all cases and substantially less than that for a majority of cases examined.

- A comprehensive, high-resolution, set of velocity and vorticity field measurements clearly show the presence of well-organized, strong, streamwise vortices with the activation of microjets. By considering the results of the 2 and 3-component PIV measurements in terms of the vorticity transport equation, there is very strong circumstantial evidence that the streamwise vorticity is primarily due to the redirection of the azimuthal vorticity in the primary shear layer.
- It appears that microjet control strategy is so successful because it disrupts the feedback loop in a number of ways; i) Through the weakening of the azimuthal vorticity by the generation of streamwise vorticity; ii) The activation of microjets also disrupts the spatial coherence of the interaction between the acoustic waves and the instability wave in the primary jet shear layer.
- A physical model was developed which appears to capture the essential features of the impinging jet flowfield from a controls' perspective.
- An in-house actuator was designed so that the microjets can be temporally modulated thus allowing for more efficient implementation of close-loop control. This significantly improved control effectiveness by providing larger or comparable noise reductions relative to steady microjets with significantly less mass flow rate.
- Initial experiments with hot impinging jets demonstrate that although the feedback loop may be more dominant for hot jets, microjet control is equally, if not more, in controlling hot jets.

10. REFERENCES

1. Alvi, F. S., Ladd, J. A. and Bower, W. W. "Experimental & Computational Investigation of Supersonic Impinging Jets," *AIAA Journal*, vol. 40, No. 5, May 2002.
2. Alvi, F. S., Elavarasan, R. and Shih, C. Garg. G. and Krothapalli, A., "Active Control of Supersonic Impinging Jets Using Microjets," *AIAA Journal*, Vol. 41, No. 7, July 2003, pp. 1347-1355.
3. Choi, J., Annaswamy, A. M., Egungwu, O., and Alvi, F. S., \Active Noise Control of Supersonic Impinging Jet Using Pulsed Microjets," 2005-798, AIAA paper, 2005.
4. Choi, J., Wee,. D., Annaswamy and Alvi, F. S., "Active Noise Control of Supersonic Impinging Jets Using a Physical Model," AIAA Paper 2005-2893, presented at 11th AIAA/CEAS Aeroacoustic Conference and Exhibit, Monterey, CA, June 2005.
5. Elavarasan, R., Krothapalli, A., Venkatakrishnan, L., and Lourenco, L., "Suppression of Self-Sustained Oscillations in a Supersonic Impinging Jet", *AIAA Journal*, Vol. 39, (12), 2001, 2366-2373.
6. Holmes, P. J., Lumley, J. L., and Berkooz, G. "Turbulence, Coherent Structures, Dynamical Systems and Symmetry," Cambridge University Press, 1996.
7. Karamcheti, K., Bauer, A.B., Shields, W.L., Stegen, G.R., and Woolley, J.P., "Some Features of an Edge Tone Flow Field", NASA SP 207, 1969, pp. 275-304.
8. Kim, J.H. and Samimy, M. 1999 Mixing enhancement via nozzle trailing edge modifications in a high speed rectangular jet. *Phys. of Fluids,* **11,** 2731.
9. Krothapalli A., Strykowski P. J. and King C. J., "Origin of Streamwise Vortices in Supersonic Jets," *AIAA Journal*, Vol. 36: No. 5, 1998, pp. 869-872.
10. Krothapalli, A., Rajakuperan, E., Alvi, F., and Lourenco, L., "Flow Field and Noise Characteristics of a Supersonic Impinging Jet", *J. Fluid Mechanics*, **392**, 1999, pp. 155-181.
11. Lou, H., Alvi, F. S. and Shih, C., "Active and Passive Control of Supersonic Impinging Jets," *AIAA Journal*, vol. 44 , No. 1, Jan. 2006, pp. 58-66.
12. Marble, F.E., Zukoski, E.E. and Jacobs, J. W.1990 Shock Enhancement and Control of Hypersonic Mixing and Combustion. *AIAA Paper* No. 90-1981

13. Margason, R., Arledge, T.K., Wardwell, D. A., Hange, C and Naumowicz. T., "Jet Efflux Characteristics and their Influence on STOVL Aircraft Propulsion-Induced Effects", Proceedings of International Powered Lift Conference, SAE P-306, March 1997, pp. 3-10.
14. Neuwerth, G.," Acoustic Feedback of a subsonic and Supersonic Free Jet which Impinges on an Obstacle", NASA TT F-15719, 1974.
15. Phalnikar, K. A., Alvi, F. S. and Shih, C. "Behavior of Free and Impinging Supersonic Microjets," AIAA Paper 2001-3047.
16. Powell, A., "The Sound-Producing Oscillations of Round Underexpanded Jets Impinging on Normal Plates", *J. Acoust. Soc. Am.*, 83 (2), 1988, 515-533
17. Samimy, M. Zaman, K. B. M.Q. and Reeder, M. F., "Effect of Tabs on the Flow and Noise Field of an Axisymmetric Jets," *AIAA Journal*, Vol.31, No.4, 1993, pp. 609-619.
18. Sheplak, M. and Spina, E.F., "Control of high-speed impinging-jet resonance", *AIAA Journal*, Vol.32, No.8, 1994, pp. 1583-1588.
19. Shih, C., Alvi, F. S., and Washington, D., "Effects of Counterflow on the Aeroacoustic Properties of a Supersonic Jet," *AIAA Journal of Aircraft*, Vol. 36, No. 2, March/April 1999, pp. 451-457
20. Tam, C.K.W., and Ahuja, K.K., "Theoretical model of discrete tone generation by impinging jets", *J. Fluid Mech.*, Vol. 214, 1990, pp 67-87.
21. Waitz, I.A., Marble, F.E. and Zukoski, E.E. 1992 Vorticity Generation by Contoured Wall Injectors. *AIAA Paper* No.92-3550.
22. Zaman, K. B. M.Q., Reeder, M. F. and Samimy, M. "Control of an Axisymmetric Jet Using Vortex Generators," *Physics of Fluids*, Vol. 6, No. 2, February 1994, pp. 778-793.

11. PERSONNEL SUPPORTED

Faculty

FAMU-FSU:
Assoc. Prof. F. Alvi (Ph.D., Penn State) is the PI and Profs. A. Krothapalli (Ph.D., Stanford) and C. Shih (Ph.D., USC) are Co-PI's at Florida A & M University-Florida State University (FAMU-FSU).

MIT:
Dr. A.M. Annaswamy (Ph.D., Yale), is the PI at MIT.

Students

FAMU-FSU:

- Ms. C. Davy - M.S. in Fall 2003
- Mr. O. Egungwu - MS in 2004.
- Mr. H. Lou, PhD. - summer 2005.
- Mr. M. Mathur – M.S. expected completion in summer 2006.

MIT:

- Mr. J. Choi,: MS in 2003
- Mr. J. Choi,: Ph.D. in summer, 2006.

12. PUBLICATIONS & INTERACTIONS

12.1 Related Archival Publications By Investigators (published, submitted & in preparation)

1. Kumar, V. and Alvi, F. S., "Use of High-Speed Microjets for Active Separation Control," *AIAA Journal*, vol. 44 , No. 2, Feb. 2006, pp. 273-281

2. H. Lou, C. Alvi, F. S. and Shih, C., "Active and Passive Control of Supersonic Impinging Jets," *AIAA Journal*, vol. 44 , No. 1, Jan. 2006, pp. 58-66.

3. Zhuang, N. Alvi, F. S., Alkilsar, M. and Shih, C., "Aeroacoustic Properties of Supersonic Cavity Flows and Their Control," to appear in the *AIAA Journal*, accepted for publication, (Jan 2006) anticipated publication: Summer 2006.

4. Alvi, F. S., Shih, C., Elavarasan, R., Garg, G, and Krothapalli, A., "Control of Supersonic Impinging Jets Using Supersonic Microjets", *AIAA Journal,* Vol. 41, No. 7, July 2003, pp. 1347-1355.

5. Alvi, F. S., Ladd, J. A. and Bower, W. W. "Experimental & Computational Investigation of Supersonic Impinging Jets," AIAA Journal, Vol. 40, No. 5, May 2002.

6. Choi, J., Annaswamy, A. and Alvi, F. S., "Active Control of Supersonic Impingement Tones Using Steady and Pulsed Microjets," submitted to *Experiments in Fluids*, August 2005, under review.

7. Sahoo, D., Annaswamy, A. and Alvi, F. S., "Microjets-Based Active Control of Store Trajectory in a Supersonic Cavity Using a Low-Order Model, "submitted to the *AIAA Journal*, April 2005, under review.

8. H. Lou, C., Alvi, F. S. and Shih, C., "A Closer Look at the Use of Microjets for the Control of the Unsteady Flowfield in Supersonic Impinging Jets," to be submitted to the *Journal of Fluid Mechanics*, anticipated submission date: Summer 2006.

12.2 Presentations and Conference Publications (03-05)

1. Zhuang, N. Alvi, F. S. and Shih, "Another Look at Supersonic Cavity Flows and Their Control," AIAA Paper 2005-2803, presented at 11th AIAA/CEAS Aeroacoustic Conference and Exhibit, Monterey, CA, June 2005.

2. Choi, J., Wee,. D., Annaswamy and Alvi, F. S., "Active Noise Control of Supersonic Impinging Jets Using a Physical Model," AIAA Paper 2005-2893, presented at 11th AIAA/CEAS Aeroacoustic Conference and Exhibit, Monterey, CA, June 2005.

3. Kumar, V. and Alvi, F. S., "Efficient Control of Separation using Microjes," AIAA Paper 2005- 4879, presented at the 35th AIAA Fluid Dynamics Conference and Exhibit, June 6-9, 2005, Toronto, Canada.

4. Bourgois, S.. Favier, J., Sommier, E., Tensi, J. and Alvi, F. S., "Etude Expérimentale du Contrôle des Décollements de Couche Limite par Aspiration et Soufflage," presented at the *Congrès FLUVISU11*, 'Ecole Centrale de Lyon, Lyon, France, June 7-9, 2005.

5. Alvi, F. S., C. Shih and Krothapalli, A. "Some Examples of Active Flow Control Using Microjets," Presented at the International Symposium on Recent Advances in Aeroacoustics and Active Flow-Combustion Control, Goa, January 4-6, 2005 *(invited)*

6. S. Bourgois, Alvi, F. S., J. Tensi and J-P Bonnet*, "Control of Flow Separation Using Microjets," presented at the First European Forum on Flow Control, Poitiers, France, October 11-14, 2004.

7. Choi, J., Annaswamy, A.M., Egugnwu, O. and Alvi, F. S., "Active Noise Control of Supersonic Impinging Jets Using Pulsed Microjets," AIAA Paper, presented at the 43rd AIAA Aerospace Meeting and Exihibit, Reno, Nevada, 10-13 January, 2005.

8. Sahoo, D., Annaswamy, A. M., Zhuang, N., and Alvi, F. S., "Control of Cavity Tones in Supersonic Flow," AIAA 2005-0793, presented at the 43rd AIAA Aerospace Meeting and Exihibit, Reno, Nevada, 10-13 January, 2005.

9. Cattafesta, L. N. , Alvi, F. S., Williams, D. and Rowely, C. , "Review of Active Control of Flow-Induced Cavity Oscillations," 33rd AIAA Fluid Dynamics Conference and Exhibit, 23 - 26 Jun 2003, Orlando, Florida. (Invited)

10. Kumar, V., Alvi, F. S., "Active Control Of Flow Separation Using Supersonic Microjets," ASME 2003 Fluids Engineering Meeting, July 6-10, 2003, Honolulu, Hawaii.

11. Alvi, F. S., Lou, H. and C. Shih, "A PIV Study of Supersonic Impinging Jets," 9th AIAA/CEAS Aeroacoustic Conference and Exhibit, Hilton Head, South Carolina, 12 - 14 May 2003.

12. Zhuang, N. Alvi, F. S., Shih, C., Sahoo, D. and Annaswamy, A. M, "Aeroacoustic Properties of Supersonic Cavity Flows and Their Control," AIAA 2005-0793, 9th AIAA/CEAS Aeroacoustic Conference and Exhibit, Hilton Head, South Carolina, 12 - 14 May 2003.

12.3 Technology Transition

We are a primary Boeing partner in a DARPA project on Micro Adaptive Flow Control (MAFC) where supersonic microjets are being used for active control of cavity flows at supersonic speeds. To date, the results have been very promising and microjets are the most effective actuator that also meet the overall system requirements. Further testing for cavity flow control is rapidly proceeding at Boeing, Long Beach. Full-scale tests using supersonic microjets are scheduled to take place in the summer of 2006 under Phase III of the DARPA project. The microjets are also one of the primary actuators in an AFRL sponsored project for cavity flow control for the Long Range Strike Aircraft (LRSA). Microjets have also been used very successfully in reducing jet noise emanating cold and hot supersonic jets under work sponsored by the Office of Naval Research; this research shows considerable promise for transition to an aircraft platform. In research sponsored by NASA Langley under the Ultra Efficient Engine Technology (UEET) initiative, supersonic microjets are also being evaluated for separation control in adverse pressure gradients, such those which occur in inlet diffusers and S-ducts. The results to date have been very encouraging in that microjets have been shown to eliminate or delay separation over a range of conditions.

12.4 New Discoveries, Inventions or Patent Disclosures Related to this Work

- A utility patent was granted on the use of microjets for controlling supersonic impinging jets; **Patent number** *6,837,456*
- A provisional patent application was filed on the use of microjets in cavity flow control. – **Patent Pending, No.** *60/575,537*